The Triplex BioValsalva Prostheses To Reconstruct the Aortic Valve and the Aortic Root

Yijun Fu,[a] Bin Li,[b,c,d] Jean Michel Bourget,[b,c] Olexandr Bondarenko,[b,c] Jing Lin,[a] Randolph Guzman,[e] Royston Paynter,[f] Denis Desaulniers,[b] Boyin Qin,[g] Lu Wang,[a] Lucie Germain,[b, c] Ze Zhang,[b, c] & Robert Guidoin[b, c]

[a]Key Laboratory of Textile Science and Technology of the Ministry of Education, College of Textiles Donghua University, Shanghai, China; [b]Department of Surgery, Faculty of Medicine, Laval University, Québec, QC, Canada; [c]Division of Regenerative Medicine, CHU de Québec Research Centre, Québec, QC, Canada; [d]Department of Peripheral Angiopathy, Shanghai Traditional Chinese Medicine (TCM) Integrated Hospital, Shanghai, China; [e]Vascular Surgery, St. Boniface General Hospital and Department of Surgery, University of Manitoba Winnipeg, MB, Canada; [f]INRS, Energie, Materiaux et Communications, Varennes, QC Canada; [g]Shanghai Public Health Clinical Center, Fudan University, Shanghai, China

*Address all correspondence to: Robert Guidoin, PhD, Department of Surgery, Faculty of Medicine, Vandry Building, Room 4873, Laval University, Québec QC G1V 0A6 Canada; E-mail: robert.guidoin@fmed.ulaval.ca

ABSTRACT: The Bentall procedure introduced in 1968 represents an undisputed cure to treat multiple pathologies involving the aortic valve and the ascending thoracic aorta. Over the years, multiple modifications have been introduced as well as a standardized approach to the operation with the goal to prevent long-term adverse events. The BioValsalva prosthesis provides a novel manner to more efficiently reconstruct the aortic valve together with the anatomy of the aortic root with the implantation of a valved conduit. This prosthesis comprises three sections: the collar supporting the valve; the skirt mimicking the Valsalva, which is suitable for the anastomoses with the coronary arteries; and the main body of the graft, which is designed to replace the ascending aorta. The BioValsalva prosthesis allows the Bentall operation to be used in patients whose aortic valve cannot be spared.

KEY WORDS: BioValsalva, Bentall, aortic root, aortic valve, type A dissection, aneurysm

I. INTRODUCTION

The Bentall procedure is a cardiac surgery involving the aortic valve (either repair or replacement), the aortic root, and the ascending aorta, with reimplantation of the coronary arteries. This procedure was first described by Bentall and De Bono in 1968 and is now commonly used to cure a wide spectrum of pathologic conditions involving both the aortic valve and the ascending aorta.[1] This procedure is generally necessary in cases of tissue lost, aneurysmal degeneration, acute dissection, aortic stenosis with small root, and porcelain aorta.[2] Over the years, surgeons have proposed multiple modifications to the original technique in response to adverse events.[3–5] The valve-sparing procedure proposed by David became widely accepted because the reimplantation technique allowed preservation of the aortic valve.[6,7] In 1980, Kouchoukos et al. recommended the open-button technique to prevent the formation of pseudo-aneurysms at the site of coronary anastomosis.[8] This technique was further modified by Michialon et al. in 2001 to prevent the valve graft from tearing and to reduce coronary button anastomosis tension.[9] In 2007, Albertini et al. recommended the double sewing-ring technique to simplify reoperation due to valve degeneration.[10] The benefits of selecting homografts were seriously hampered by the difficulties of procurement.[11–13] Other devices manufactured with chemically treated biological tissues showed interesting possibilities but remained marginal.[14–17] Adverse events were frequently related to the stress at the anastomoses with the coronary arteries.[18–22] These multiple innovations were designed with the intent to minimize recognized complications but did not result in a real consensus.[23–26] The Bentall operation, with the implantation of a prosthetic valve (bioprosthesis or mechanical valve), became the

most accepted procedure;[27] however, many questions emerged.[28,29] Based on sound clinical experience, De Paulis developed a prosthesis to make this surgical technique more accessible and to maximize the durability of the procedure.[30–32] The BioValsalva consists of tubular fabrics valves with bioprostheses fitted in a Triplex conduit.[33–35] We hereby report our analyses of the Triplex BioValsalva valve prostheses to reconstruct the aortic valve and the aortic root.

II. MATERIALS AND METHODS

A. Devices

Two Triplex BioValsalva prostheses—one stented, one non-stented—were investigated. These devices were manufactured by Vascutek, a Terumo Company (Inchinnan, Scotland, UK), based on research conducted by De Paulis et al. to more consistently repair and replace the aortic valve together with the pathological ascending thoracic aorta (e.g., aneurysm, dissection, or coarctation).[21] The Triplex BioValsalva device consisted of three sections: a collar, a skirt, and a body. The collar of the first device supported a stented porcine valve, whereas the collar of the second supported a non-stented valve. In both devices, the fabric was a self-sealing graft material called Triplex that consists of three layers: inner woven polyester, central SEPS (styrene ethylene propylene styrene block copolymer, a thermoplastic elastomer), and an outer PTFE coating.[35,36] This fabric conduit is similar to the Valsalva that has been investigated previously.[37] However, in this device, zero water permeability was achieved with a degradable gelatin coating.[38] The selected porcine bioprostheses were the Elan Vascutek-Terumo, stented and nonstented, whose respective performances have been reported previously.[39,40]

B. Testing

1. Non-Destructive Testing

Gross observations were performed on the devices as received from the manufacturer. To identify any flaws, photographs were taken using a digital camera (Song DSC F707, 5 megapixels). The images

were processed with Adobe Photoshop CS4. A polyester, 4-mm-diameter graft was anastomosed to the Valsalva of the unstented BioValsalva device in our laboratory after a 4-mm-diameter hole was cut in the wall using a surgical blade. The skirt was punctured using a trocar to mimic the air purge before restoring the blood flow.

For micro-computed tomography (Micro-CT) investigations, the devices were placed on the examination bed (width, 75 mm) of the eXplore Locus Micro-CT Scanner (GE Healthcare, London, Ontario, Canada) and set on the rotating stage. X-ray settings of 80 kV and 450 μA were applied to the devices over 360° rotation, with an exposure time of 100 ms per frame. The effective pixel size was 92 μm. The scanner produced a 2D projection image in 0.9° angular increments around the device, resulting in 400 views with 10 min scanning time. The 2D projections were reconstructed at a 3D volume using a modified Feldkamp cone-beam algorithm to allow voxel-driven convolution and back projection. The 400 views were reconstructed and analyzed using Reconstruction Utility software and eXplore MicroView v. 2.0 (GE Healthcare, Madison, WI).

2. Destructive Testing: Histology of the Bioprostheses

Tissue samples (3 to 5 mm wide, 1 cm long) were dissected from each leaflet of each prosthesis and processed for scanning electron microscopy, light microscopy, and transmission electron microscopy.

Scanning electron microscopy studies were conducted as follows: After post-fixation in a 1% osmium tetroxide, the specimens were rinsed in distilled water, dried in ethanol solutions of graded concentrations until the use of absolute ethanol and transferred in absolute acetone. Final drying was achieved in hemaxamethyldisilazane. After gold-palladium coating, (Sputter Coater Nanotech Semprep2 Nano-Tech Burton on Trent, UK), the specimens were observed by scanning electron microscopy (Jeol, JSM-6360LV, Jeol, Tokyo, Japan) at accelerating voltages ranging from 15 kV to 25kV.

For light microscopy, the specimens were embedded in paraffin, cut in 5-μm-thick slides using a microtome. Sections were stained with hematoxy-

lin and eosin (HE) for general observation using a polarized microscope; with Masson's trichrome for the visualization of collagen; with Weighert and Verhoeff for visualization of elastic fibers; and with red picrosirius for examining the waviness of the collagen bundles. The slides were observed in Axio Imager M2 (Zeiss, Jena, Germany), and the photos were processed with the Axio Vision Release 4.2.2 progiciel.

Transmission electron microscopy was conducted as follows: After post-fixation in 1% osmium tetroxide solution followed by uranylacetate staining, specimens were embedded in Epon and cut in thin sections using an ultramicrotome. Following additional lead citrate and uranylacetate staining, the samples were observed by transmission electron microscopy at a voltage of 80 kV in a Jeol JEM 1230.

3. Destructive Testing: Fabric

The fabric analysis was based on the recommendations of the ISO 7198-1998 for tubular vascular prosthesis[41] and was adapted from the protocols that we previously used for testing fabric conduits.[42–44]

For dissection of the device and related observations, each device was opened longitudinally and divided into two identical halves to be photographed with a digital camera. Each specimen was observed using light microscopy under a 10× magnification before and after elimination of the outer elastomer layer. The fabric and its coating were boiled for 10 minutes in a 99.5% solution of cyclohexanone ($C_6H_{10}O$). After cooling overnight at room temperature, the specimens were rinsed twice in distilled water and air dried. Each specimen was observed under 10× magnification to confirm the complete removal of the coating. If any trace was found, the procedure was repeated.

Morphology of the walls of the different sections of Valsalva graft, before and after removing the coating, were determined as follows: Using light microscopy, the specimens were observed with a PXS8-T optical compound microscope (Shanghai Cewei Photoelectric Technology, Shanghai, China) with CCD of Nikon Digital Sight DS.Fil (Nikon Imaging, Shanghai, China) fitted with an eyepiece

scale at a ×10 magnification. For scanning electron microscopy, the fabric specimens (0.5×0.5 cm^2) were made conductive by sputter coating with platinum and examined in a Jeol JSM-5600LV environmental scanning electron microscope at an accelerating voltage of 15 kV.

Structures of the woven fabrics were observed with a light microscope. The pattern of the fabrics was drawn according to the observations using the following measurements. For the fabric count, the number of ends and picks per unit in the woven fabric were measured at 40× magnification. The number of ends and picks within 1 mm was counted using MB-Ruler software. Twenty locations were randomly selected on each fabric specimen to obtain the mean value and standard deviation.

To determine thickness, a thickness gauge model CH-12.7-BTSX (Shanghai Liuling Instrument, Shanghai, China) with a minimum division of 0.001 mm was employed to measure the fabric thickness after cleaning. The diameter of the columniform gauge head is 5 mm; the area of the presser foot is 19.63 mm^2; and the testing pressure is 22±5 KPa (44±10 g). Ten different locations were randomly selected for each specimen.

The mass of the fabric specimens was measured with an electronic analytical balance model FA2004 (Shanghai Liangping Instrument, Shanghai, China) with 0.1-mg resolution. Specimens of 1×1 cm^2 in size were selected at three locations on both cleaned fabrics. Each specimen was measured five times to calculate the mean and standard deviation. The mass per unit area (g/cm^2) of the fabric specimens was then determined.

The porosity (P) of the fabric, i.e., the volume of the void space as a proportion of the total volume of the fabric, was calculated as follows:

$$P = 100 \text{ X } (1 \text{ X } \frac{M}{t\rho}$$

where M is the mass per unit area (g/cm^2), t is the thickness in centimeters, and ρ is the density (1.38 g/cm^3) of the polyester fibers.

To determine the number of filaments in each yarn, the three types of yarns in each fabric (i.e., upper warp yarns, inner warp yarns, and weft yarns)

were separated from ten different locations with tweezers under a magnifier. The number of the filaments in each yarn was counted three times to guarantee the accuracy of the count. Special attention was aimed toward avoiding yarn breakage and fiber entanglement during the procedure.

To determine the filament diameters, individual filaments were removed, and their diameters were determined using a light microscope model CH-2 (Nikon Imaging) at a magnification of 400×. MB-Ruler software was employed to precisely measure the diameter of the filaments. Each filament was gauged 50 times to determine the mean and standard deviation.

Linear density of yarns and filaments, i.e., mass per unit length of fibers or yarns, was determined in decitex (dtex), i.e., the mass in decigrams per kilometer of yarn or fiber. The nominal linear density was calculated using the following equation:

$$d(dtex) = \frac{n}{100} \times \frac{\pi D^2}{4} \rho$$

where ρ is the density (1.38g/cm³) of polyester fibers, D is the average filament diameter in micrometers, and is n the number of filaments in each yarn.

To assess the mechanical performances of the filaments, 20 individual filaments were pulled from both warp and weft yarns selected from ten different locations of the fabric specimens. Special attention was aimed toward preventing any accidental tension imposed on the fiber likely to make the measurements inaccurate. A fiber tensile tester model XQ-2 (Shanghai Lipu Applied Science and Technology Research Institute, Shanghai, China) was used to test the tensile performances of the filaments at a stretching speed of 10 mm/min with a pre-tension of 0.75cN/dtex and a clamping distance of 10 mm. For each type of filament, the test was repeated 20 times to calculate the average and standard deviation.

The surface chemistry was first examined in an X-ray photoelectron spectroscope (XPS). The survey analysis of the surface elemental composition was performed on the different sections of the blood conduits, i.e., the skirt and the body. The coupons were selected in the devices as received and after cleaning i.e., digestion of the external layer (SEPS with the outer PTFE layer). The analyses were conducted using a Thermo VG 200iXL (VG Sientia, Newburg Port, MA, USA) with a non-monochromatized AlKα source without charge compensation.

The surface chemistry of the BioValsalva fabric was also examined using a Fourier transform infrared imaging microscope (FTIR-IM) model Nicolet IN 10MX (Thermo Fisher Scientific, Waltham, MA, USA) and was compared to the surface of the polyester fabric after digestion of the self-sealing polymer. The specimens were flattened and pressed against the crystal prism of the attenuated total internal reflectance (ATR) system to observe the absorption bands. The spectra were analyzed using proprietary software Omnic V 6.0.

Using differential scanning calorimetry (DSC), the thermal properties of the blood conduit from the explant and the control were measured (Model 204F1, Netzsh Scientific Instruments, Shanghai, China). Specimens of approximatively 3–4 mg each were cut and loaded into aluminum pans and sealed. The pans were heated from 50°C to 300°C at the same heating rate. The data were collected and analyzed with the Proteus thermal analysis software to calculate the onset and peak temperatures, heat of fusion, crystallinity, and glass transition temperature (Tg) of all endotherms and exotherms.

III. RESULTS

A. Gross Observations

The BioValsalva prostheses possessed the elements necessary to perform the Bentall operation with a valved conduit: the three sections of the devices were well differentiated (Figures 1 and 2). The porcine bioprostheses, either unstented or stented, were fixed at the collar. The second section, by the name of the skirt, was belly shaped to permit the anastomosis of the coronary arteries without tension. It mimicked the Valsalva and thus could reduce the risk of false aneurysms at the suture lines of the coronary conduits. The third section was defined as the body to serve as the outflow of the device. The crimps were perpendicular to the blood flow. This section could be trimmed by the surgeon to fit in the site of implantation. The anastomoses between the different sections were regular without any
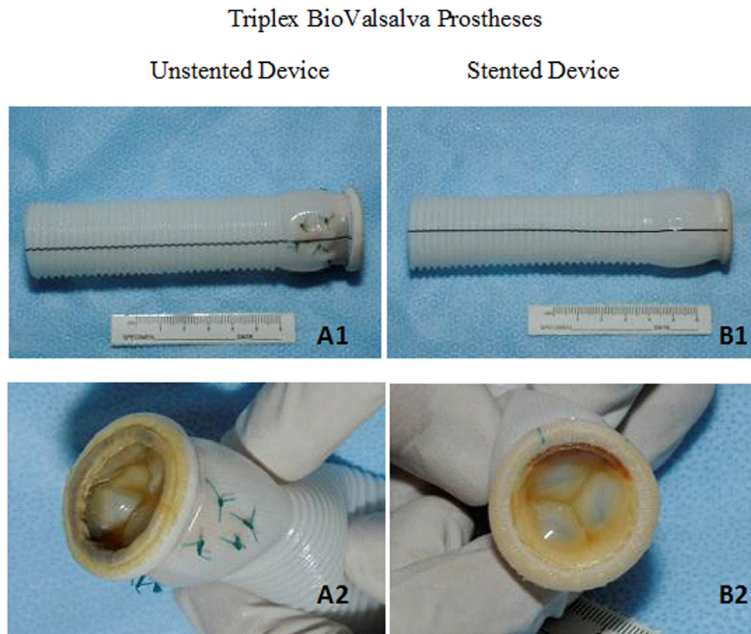
Triplex BioValsalva Prostheses

Unstented Device   **Stented Device**

FIG. 1: Gross observation of the BioValsalva prostheses. Each device (A1, B1) holds three sections, the collar supporting the valve, the Valsalva and the skirt. The Valsalva is belly shaped to anastomose the coronary conduit with reduced tension whereas the skirt is crimped perpendicularly to the blood flow. The valves are bioprostheses made of porcine aortic valve. In the unstented device, the porcine valve is scalloped and immobilized with sutures attached to the Valsalva (A2) in addition to the fixation to the collar. In the stented device the valve is only attached at the collar (B2).

Unstented Triplex BioValsalva prosthesis
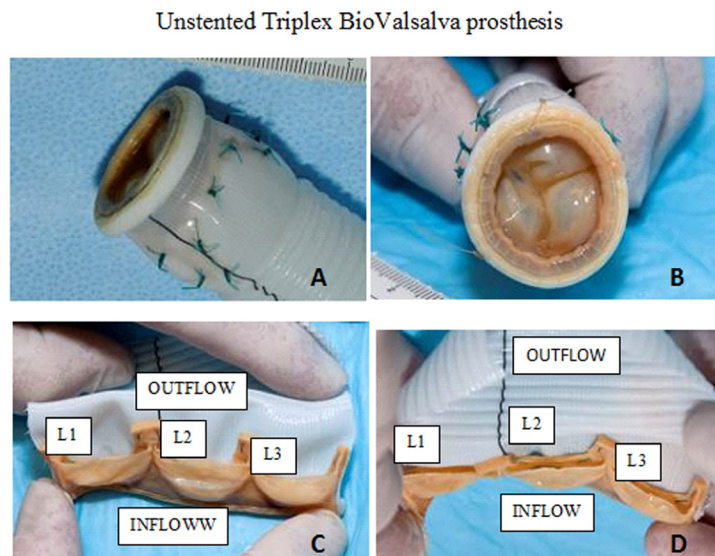
FIG. 2: Gross observation of the porcine valve in the unstented BioValsalva device. The bioprosthesis that is scalloped in the aorta is anastomosed to the collar and sutured to the Valsalva (A). The leaflets show a good cooptation (B) and the semilunar leaflets or cusps are attached to the aorta and are flawless. They can be identified as left coronary (L1), non-coronary (L2) and right coronary (L3).

Suturing a coronary conduit to the stented Triplex BioValsalva prosthesis

FIG. 3: Suturing a coronary conduit to the Valsalva to mimic the anastomosis of a coronary graft. A 4-mm spirally supported polyester graft is anastomosed with a 6.0 monofilament polypropylene suture after opening a 4-mm-diameter orifice in the Valsalva (A). The anastomosis can be completed (B), without any adverse effect on the leaflet cooptation. In addition (C) no fraying of the fabric can be seen.

fraying of the woven fabric. When observed with the naked eye, all the sections of the prostheses appeared flawless.

The suture of a coronary polyester conduit was easily performed by means of a monofilament polypropylene suture and the anastomosis did not show any fraying of the structure. The perforation of the body by means of a trocar to mimic the degasing showed some mild fraying but the hole did not stretch. Such a hole can be repaired by a single suture stitch (Figures 3-5). The valves were flawless as it was confirmed in Micro CT Scan observation (Figure 6). A good placement of the commissures of the leaflets was observed with a complete juxtaposition along their entire length. These commissures

were soft. No hematoma within the leaflets or the septal shelf was evidenced.

B. Destructive Analyses: Histology of the Valves

1. Scanning Electron Microscopy

The leaflets of the unstented BioValsalva showed a smooth surface on the inflow side (ventricular). The subendothelial layer was devoid of any endothelial cells because they were eliminated during the processing. At higher magnification, the flow surface was corrugated according to the morphology of the underneath layers of elastin fibers and waved col-
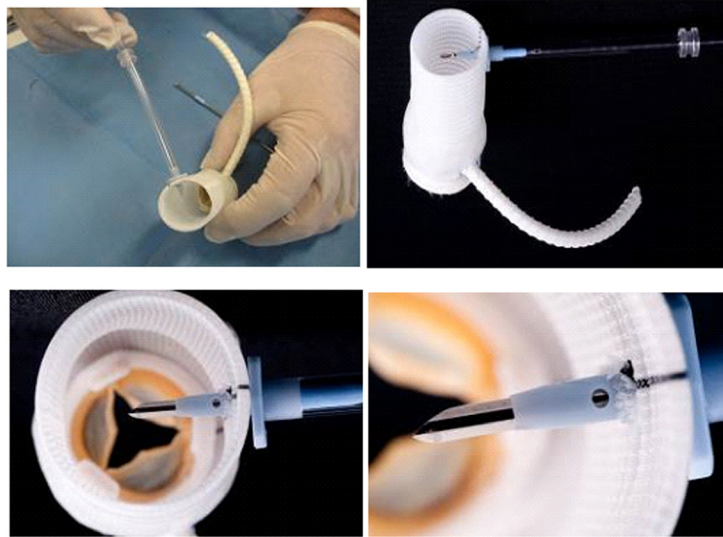
Inserting the trocar for simulation of degasing

FIG. 4: Insertion of trocar through the wall of the skirt of the stented device to permit complete degassing of the extracorporeal circuit before restoring the blood flow (A, B). The mild trauma caused by this procedure can be revised by means of a simple suturing after the trocar is pulled out (C, D).

Stented Triplex BioValsalva Prosthesis:
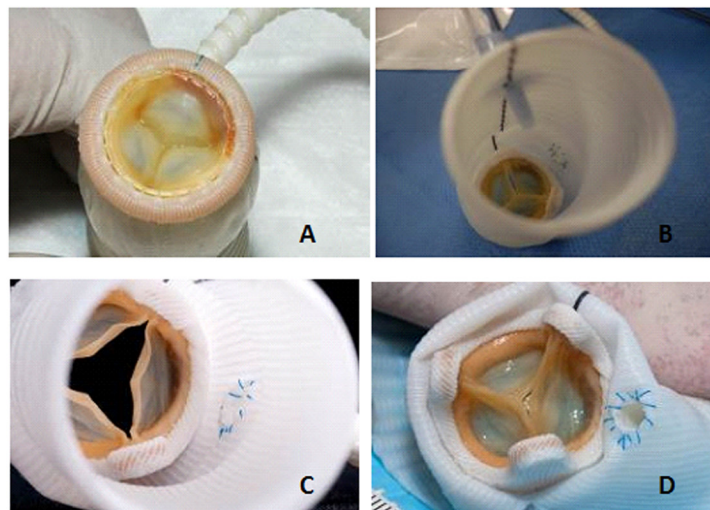
Anastomosis of the coronary conduit

FIG. 5: Anastomosis of a coronary conduit to the stented BioValsalva. The inflow shows a perfect cooptation of the three leaflets (A). The outflows together with the ostia of the coronary conduit are observed within the Valsalva (B). The valve can open as observed on the outflow side without fraying of the fabric at the ostia with the coronary conduit (C). A more detailed observation confirms the feasibility of the procedure (D).

lagen bundles. The outflow (fibrosa) was frequently somewhat crimped or corrugated. This crimped configuration corresponded to the fixation during the systole as the result of the contraction of the underneath structure of the collagen wavy crimps. The few shallow fractures on the surface were probably an artifact caused by the flattening of the sample of the specimen on the stub. The marks of the surgical tools used to suture the valve to the skirt were evidenced. This trauma was only a surface phenomenon (Figures 7–9).

The flawed surface of the leaflets of the stented BioValsalva showed a similar morphology, but there was no mark of the surgical tweezers on their surfaces (Figures 10–12).
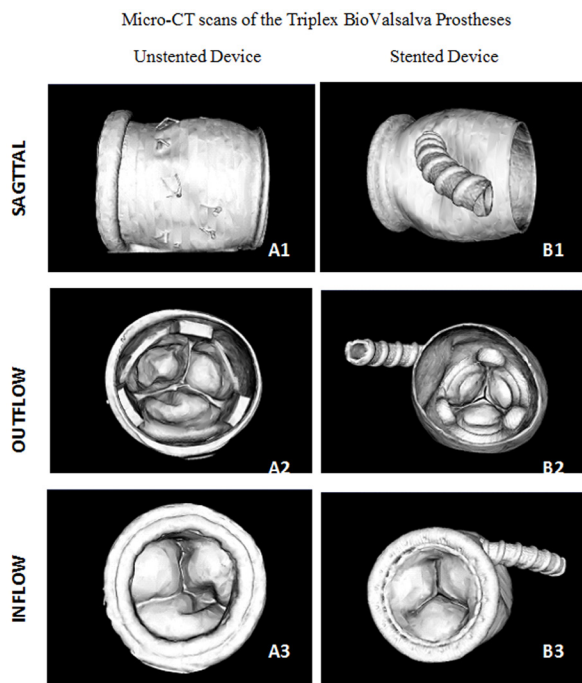
FIG. 6: Micro CT scan observation of the stented device after suturing a coronary graft (left) and the unstented device (right). The coronary branch is anastomosed to the Valsalva of the first one (A1), whereas the scalloped aortic valve is sutured to the Valsalva (B1). The co-optations at the inflow of the leaflets of both valves are adequate in both devices (A2, B2). The observations of the outflow are similar (A3, B3).
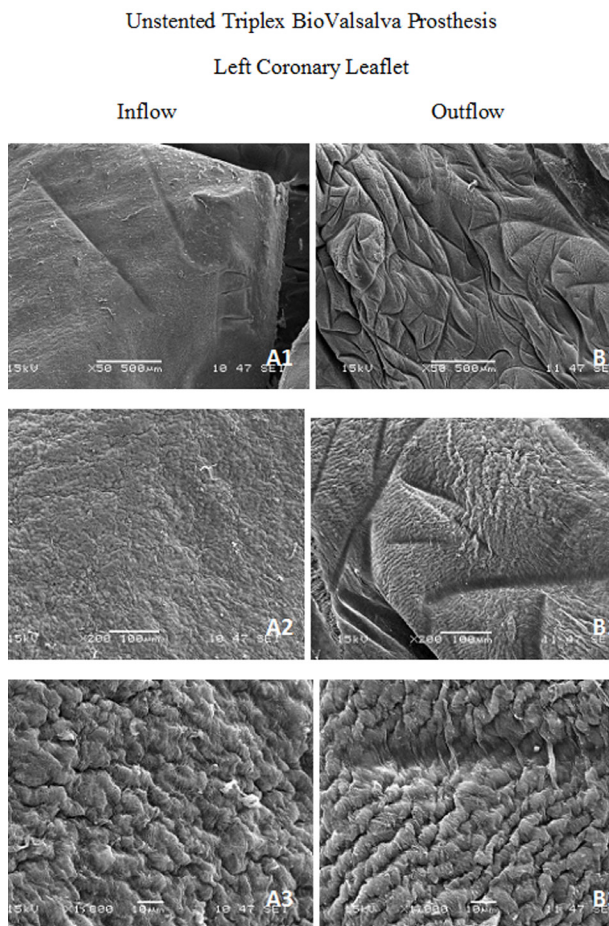

FIG. 7: Leaflet 1 in the unstented BioValsalva device. The inflow is smooth with a corrugated smooth surface with minor irregularities (A1). The subendothelial layer is continuous and devoid of endothelial cells previously eliminated during the processing. The shallow undulations follows the underneath structures of the waviness of the collagen and elastic fibers (A2,A3). The outflow shows an irregularity undulated surface with prints resulting from the handling of the valve during suturing (B1). The surface is mildly damaged with undulations following the structures of the underlying collagen bundles in addition to the corrugations at the systole (B2). At higher magnification, the subendothelial layer is shown continuous and regular (B3).

2. Light Aicroscopy

The section through the leaflets showed three layers: the lamina ventricularis at the inflow and the lamina fibrosa at the outflow with the lamina fibrosa

in between. These layers had a complex architecture designed to accommodate the repetitive changes during opening (systole) and closing (diastole). In the ventricularis, elastin and collagen showed various levels of stretching and waviness because they extended during the systole. The fibrosa frequently showed a corrugated structure because of the underneath bundles of collagen that stretches during the diastole to maintain coaptation and prevent any
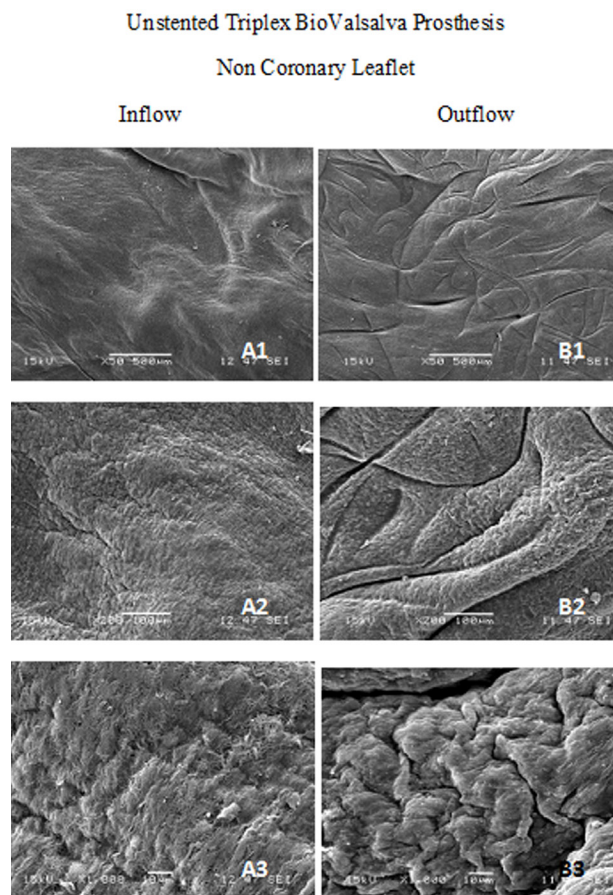
Unstented Triplex BioValsalva Prosthesis

Non Coronary Leaflet

Inflow Outflow

FIG. 8: Non-coronary leaflet in the unstented BioValsalva. The inflow side does not show the same smoothness (A1), but the subendothelium is well preserved and continuous (A2); some ghost cells are suspected (A3). The outflow shows many prints of surgical tools that applied pressure on the mildly corrugated valve (B1). The fractures in the subendothelial were aggravated by the immobilization of the tissues on the stub for observation in SEM (B2). The underneath bundles of collagen show waviness. The fibers are well differentiated (B3).
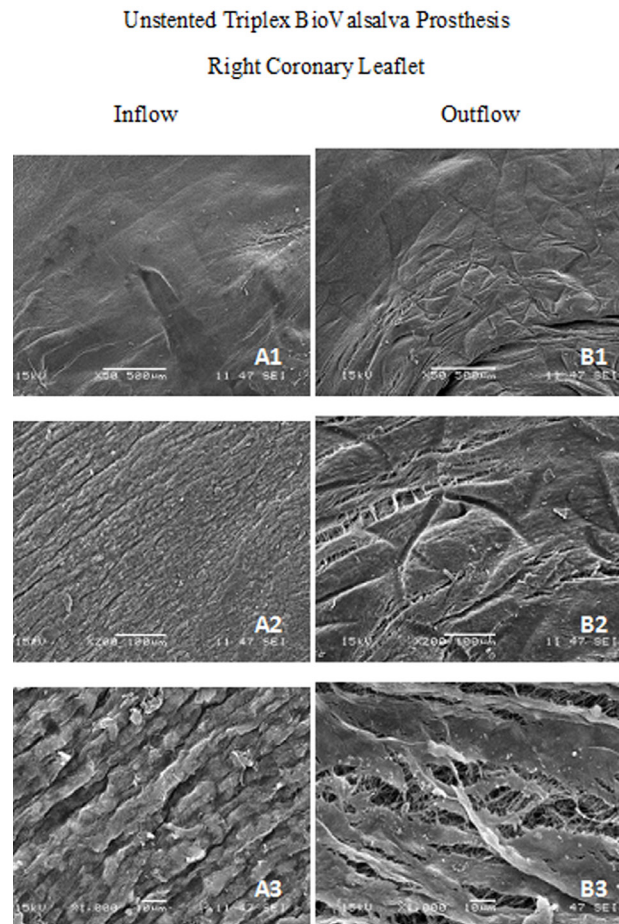
Unstented Triplex BioValsalva Prosthesis

Right Coronary Leaflet

Inflow Outflow

FIG. 9: Right coronary leaflet in the unstented BioValsalva. The inflow side is smooth but not flat and holds local belly configurations (A1). The subendothelial layer is continuous without any fracture (A2, A3). The outflow side shows a corrugated structure with longitudinal disruptions in the direction of the corrugations and the marks of surgical tools (B1, B2). The collagen bundles are visible underneath the disruption in the subendothelium (B3).

aortic leak are retracted during the systole. The spongiosa, frequently the thickest layer composed of loosely arranged collagen and abundant glycosoaminoglycans (GACs). All three layers incorporated large amounts of interstitial cells. The fibrosa involved the formation of an important member of protuberances. Both ventricular and fibrosa in their non-appositional areas and the free margins together with the spongiosa were accompanied by a significant presence of intersticial cells. The observations
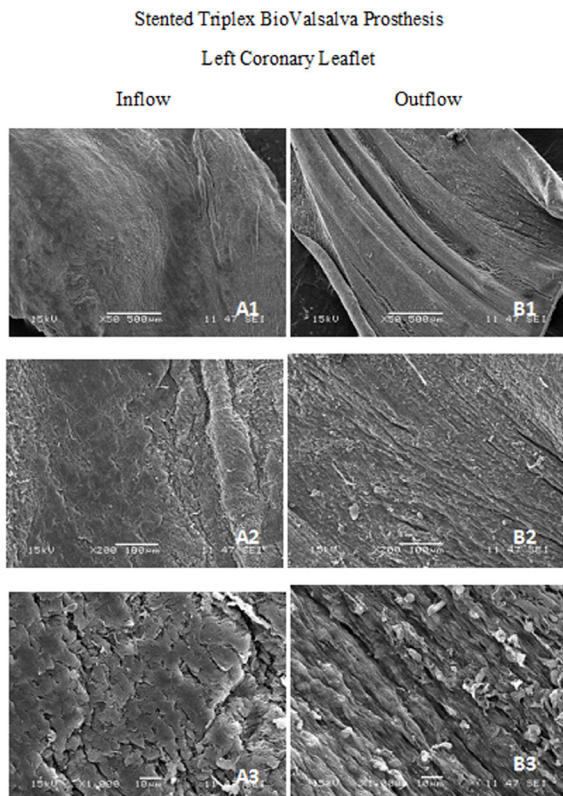
Stented Triplex BioValsalva Prosthesis

Left Coronary Leaflet

Inflow   Outflow

FIG. 10: Leaflet 1 in the stented BioValsalva device. The inflow is smooth with smooth, low-profile belly undulation (A1). The subendothelial layer is well preserved and follows the morphology of the underneath waviness of the collagen bundles (A2). The outflow is waved with disruptions parallel to the folds (B1). The fissures are aggravated by the immobilization of the sample on the stub after drying (B2). The subendothelial layer splits permit to locally identify the underlying fibers. It holds ghost endothelial cells (B3).

in the unstented prosthesis were similar to those in the stented prosthesis (Figures 13–18).

3. *Transmission Electron Microscopy*

In both, unstented and stented BioValsalva devices, the leaflets showed a great variability in the content in collagen bundles. There were empty spaces between the cells and the collagen. The collagen bundles showed waviness whatever the quantity of collagen fibers in each bundle. These fibers were never agglutinated; they were totally individualized. In addition, the characteristic banding of collagen

filaments was always visible and clearly identified on every single collagen fibril (Figures 19–24).

C. Destructive Analyses: Textile Investigations

The scanning electron microscopy photos of the blood conduits taken before eliminating the Triplex coating confirmed the complete imperviousness of the prosthetic walls in the different sections (Figure
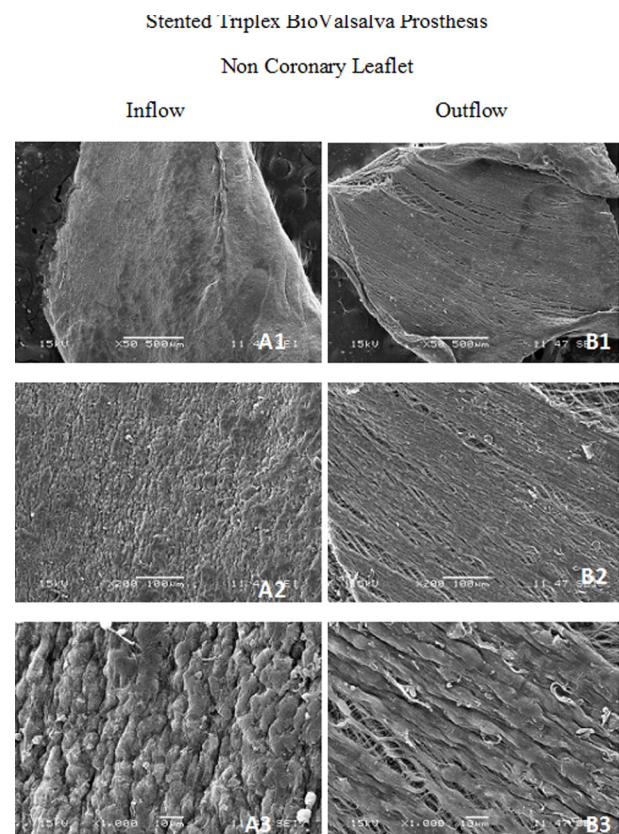

Stented Triplex BioValsalva Prosthesis

Non Coronary Leaflet

Inflow   Outflow

FIG. 11: Non coronary leaflet in the stented BioValsalva device. The inflow shows a smooth and continuous subendothelial surface with some moderately low-profile swollen areas (A1). There is no disruption in this subendothelial layer (A2) whose microstructure follows the underneath structure of the collagen bundles (A3). The outflow holds a major corrugation with longitudinal splits in the subendothelial layer parallel to this corrugation (B1). These fissures permit to visualize the underlying bundles of collagen (B2). The ghosts of endothelial cells from the endothelium are visible (B3).
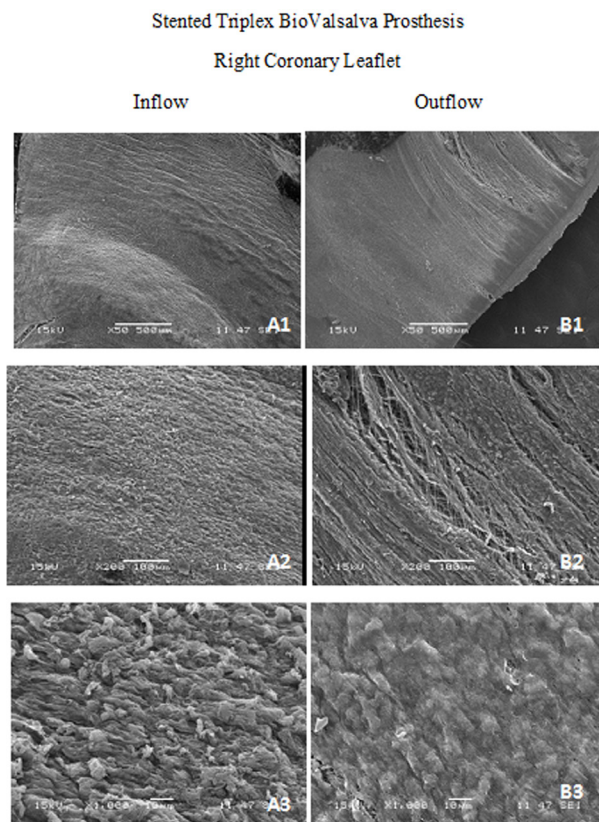
system of weft. The back warps interweave with the wefts to form the back weave, which was 1-warp/1-weft, namely plain weave, while the face warps were over the plain weave every other two warps to form
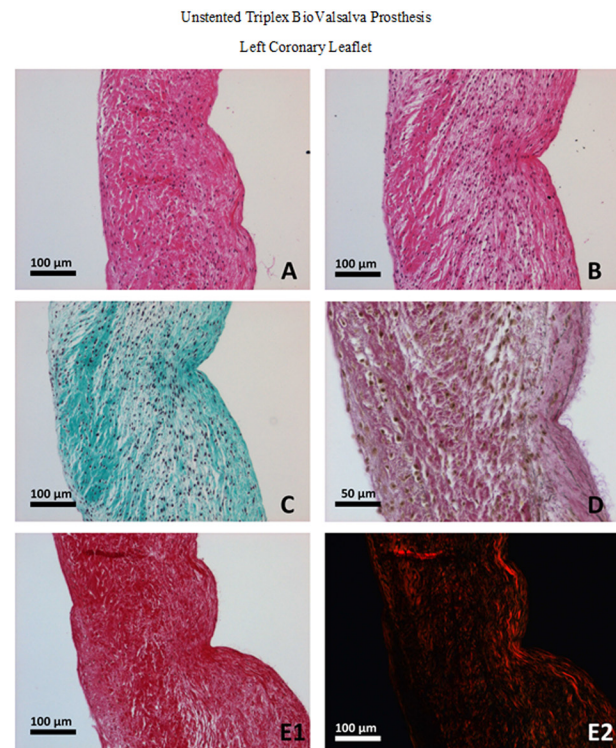

FIG. 12: Right coronary leaflet in the stented BioValsalva device. The smoothness of the outflow shows a low-profile belly structure in the vicinity of the undulations of the surface (A1). The flow surface shows some desquamation of the ghost cells of the endothelium (A2, A3). The outflow of the leaflet was locally corrugated and mostly flat (B1). The fractures in the subendothelial layer make the underlying structures of collagen bundles visible (B2). Otherwise, the surface is smooth with ghost of endothelial cells (B3).

25). The warp and weft yarns interlaced with each other to form the final structure of the fabric. The different sections were securely anastomosed with braided polyester. The anastomosis stitches were regular, and the woven structure of the fabric did not show any fraying in the unstented device or in the stented device.

1. Fabric Structure and Fabric Count

The fabric structure of the skirt and the body sections was a backed weave consisting of two systems of warp threads (face warp and back warp) and one

FIG. 13: Light microscopy photomicrographs of the left coronary leaflet of the unstented BioValsalva device. They are shown from the inflow to the outflow: the ventricularis, the spongiosa and the fibrosa. Its thickness is variable i.e., between 200 μm and 700 μm. The ventricularis, i.e., the inflow, shows bundles of collagen and elastin not organized in a specific direction. The fibrosa is the outflow, whose thickness ranges between 150 μm and 250 μm, holds large bundles of collagen that are oriented predominantly in the circumferential direction of the leaflet. It explains the frequent presence of corrugations observed in scanning electron microscopy. The fibrosa is shown as a buffer between the ventricularis and the fibrosa. It holds loosely arranged collagen and elastin fibers within the glycoaminoglycans. The endothelial cells were destroyed during the processing and thus only ghosts of endothelial cells can be observed. The subendothelium is intact without any rupture, nor fragmentation. An abundant cellularity is visible in the ventricularis and the fibrosa.
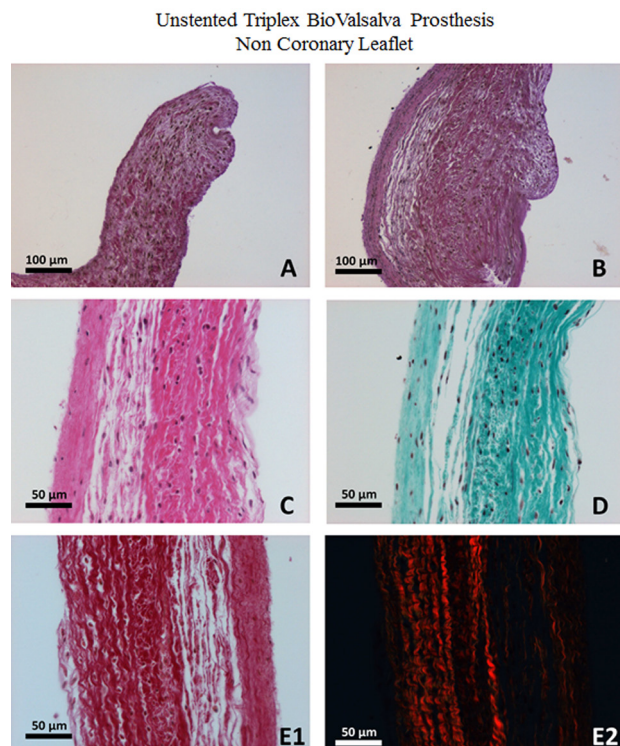
Unstented Triplex BioValsalva Prosthesis
Non Coronary Leaflet

FIG. 14: Light microscopy photomicrographs of the non-coronary leaflet of the unstented BioValsalva device at its cooptation area. The spongiosa is thinner than in Figure 13. The outflow surface, i.e., the fibrosa, is highly corrugated; this is an abundant amount of underneath collagen fibers. The outflow surface, i.e., the ventricularis, is thinner than the fibrosa and holds a large amount of collagen fibers. In both sites, the collagen bundles are parallel to the flow surface. The endothelium of both inflow and outflow holds only some ghosts of endothelial cells. The subendotheliums are intact whereas the valvular interstitial cells are dispersed in the 3 layers of the structures.

the face weave, which had three warps: 10-weft/1-warp/1-weft twill. The special warp-backed weave provided different surface aspects to the inside and outside of the fabric tube. The back weave was taken as outflow side of the tube. This structure was designed to guarantee a better support the blood pulse pressure in the human body (Figures 26–30).

2. Features of the Fabric

The thickness, mass, and porosity of the fabrics were obtained after digestion of the Triplex, i.e., specimen cleaning (Table 1). Therefore, no coating remained on the surface of the fabric. The fabric structure of the two sections in both devices was a warp-backed weave with a thickness of 0.271 mm and a mass of 0.0124 g/cm². The porosity calculated according to the value of thickness and mass after elimination of the coating was ~67%.

3. Properties of the Yarn and Filaments

The yarns in the warp direction consisted of 54 individual filaments, whereas the weft consisted of two-fold yarns holding 27 filaments each. The diameter of each individual filament was approximately 14 μm. Both the yarn linear density and
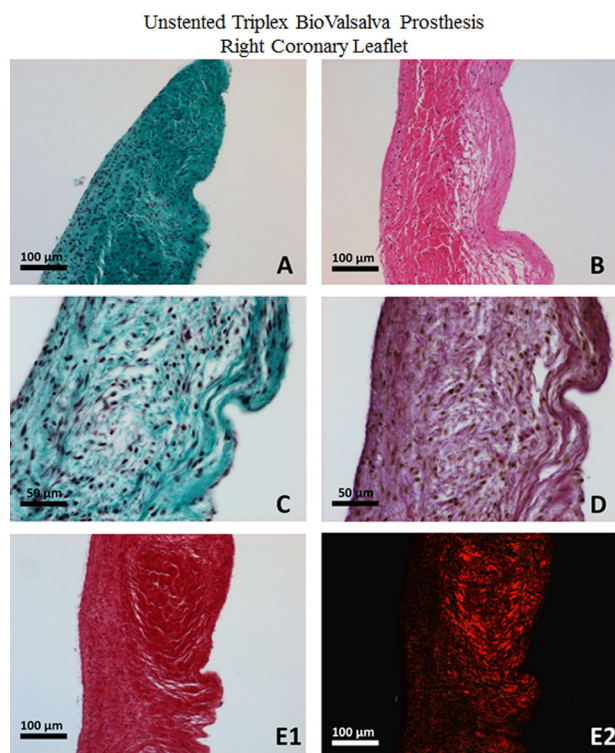
Unstented Triplex BioValsalva Prosthesis
Right Coronary Leaflet

FIG. 15: Light microscopy photomicrographs of the right coronary leaflet of the unstented BioValsalva device at its cooptation area. The profile of the fibrosa, which is thinner than the ventricularis, is highly corrugated, and the collagen bundles are oriented in various directions. The spongiosa is well identified. The valvular interstitial cells are dispersed in the ventricularis and the fibrosa, but scarce in the fibrosa.
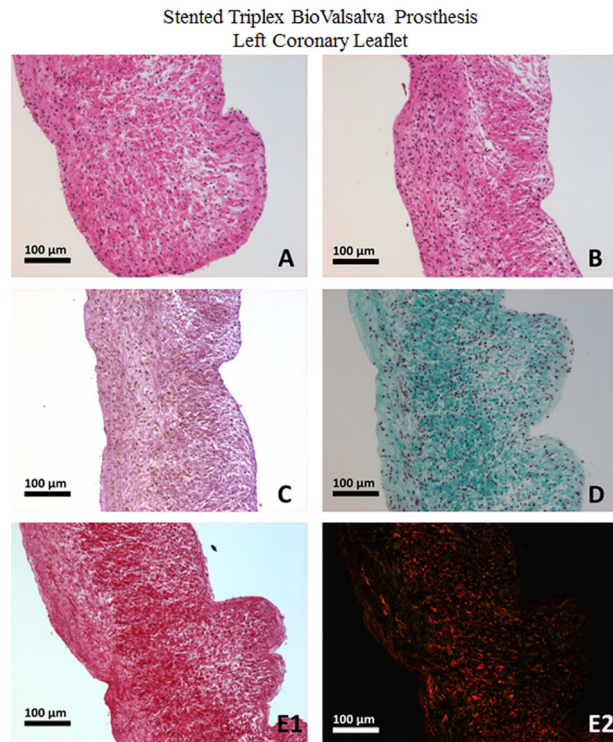
Stented Triplex BioValsalva Prosthesis
Left Coronary Leaflet

FIG. 16: Light microscopy of the left coronary leaflet of the stented BioValsalva device in the cooptation area. The spongiosa is almost absent, and the flow surface of the fibrosa is highly corrugated. The collagen bundles are oriented circumferentially. No endothelium is left, but the subendothelium layer is intact. The valvular interstitial cells are abundant throughout the cross-section.

the filament linear density were calculated values according to the measuring diameter of filament (Table 2). The stretch–strain behaviors of the filaments at both warp and weft directions of the stented and unstented fabrics are presented in Figure 31. The filaments typically exhibited a linear behavior below 3% of elongation, which likely represents the elastic deformation. Creep occurred at ~5% of elongation, followed by a long and almost linear increase of stress with strain before reaching ultimate failure between 30 and 35% of elongation. This final segment of plastic deformation is likely associated with sliding among the oriented macromolecules and stress-induced crystallization as well. All tested filaments recorded similar stress-strain behaviors except differences in the ultimate elongation.

D. Chemical Analysis

1. X-Ray Photoelectron Spectroscopy (XPS)

Table 3 lists the surface elemental composition on both sides of the stented fabrics before and after cleaning with the high-resolution C_{1s} spectra (Figure 32). Before cleaning, the inside clearly differs from outside in carbon, oxygen, and silicon contents, showing much higher oxygen and silicon contents but lower carbon content. The difference disappeared after cleaning because of the reduced oxygen and silicon on the inside. Such changes before and after cleaning were also found on the unstented fabrics (data now
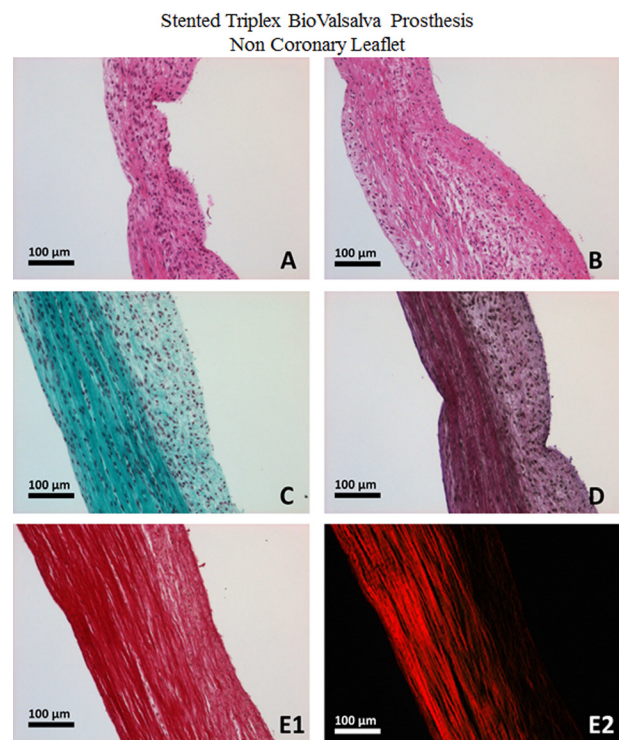
Stented Triplex BioValsalva Prosthesis
Non Coronary Leaflet

FIG. 17: Light microscopy of the non-coronary leaflet of the stented BioValsalva device in the cooptation area. The fibrosa is highly corrugated and shows various thicknesses. The spongiosa is almost absent. The ventricularis is made of stretched collagen and elastin fibers. The interstitial cells are particularly abundant in the fibrosa. There is no endothelium left, but the subendothelia are well preserved.
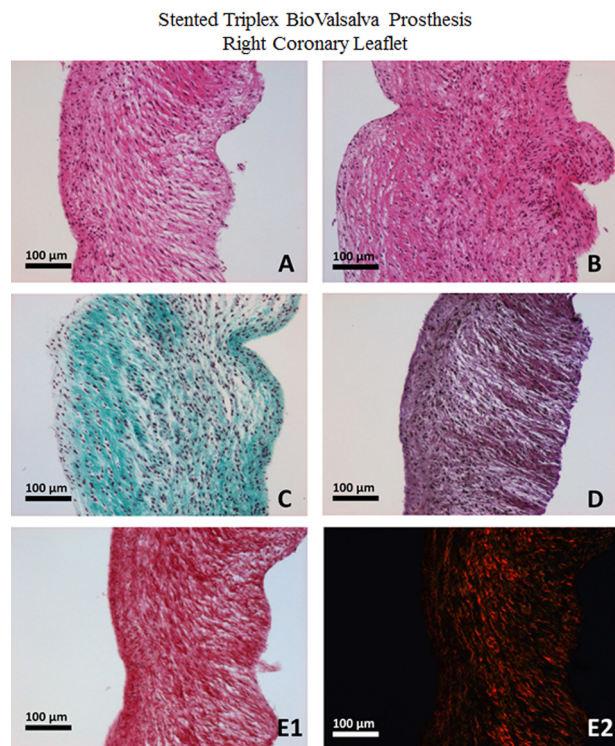
Stented Triplex BioValsalva Prosthesis
Right Coronary Leaflet

FIG. 18: Light microscopy of the right coronary leaflet of the stented BioValsalva device. The flow surface of the fibrosa is highly corrugated because of the underneath collagen bundles. The spongiosa is ill defined, whereas the collagen fibers of the ventricularis are circumferentially oriented. Abundant colonies of valvular interstitial cells are dispersed throughout the different layers of the leaflet. No endothelium is left on both the inflow and the outflow. The subendothelial layers are intact.

shown). The C_{1s} spectra inside of the fabrics before cleaning revealed distinct peaks for C-O and OC=O moieties, which almost completely disappeared after cleaning. In fact, all cleaned fabrics demonstrated similar C_{1s} spectra following cleaning, which resembled hydrocarbons with little oxygen moiety.

2. Fourier Transform Infrared (FTIR)

The FTIR results of the outside and the inside of the blood conduit of the BioValsalva prosthesis as received and after digestion of the coating are shown in Figures 33–34. The characteristic absorption spectrum of the outside of the devices as received (Figure 33a) indicated that the coating on the out-

side surface is SEPS (styrene ethylene propylene styrene block copolymer). Compared with the spectrum of the outside of the devices after elimination of the coating (Figure 34a), the conclusion that the coating has been completely removed can be drawn.

The stretching vibration of C=O group at the wave number 1,716 cm^{-1} and the stretching vibrations of C-O group at 1,247 cm^{-1} and 1,101 cm^{-1} indicated that the material of the fabric for both unstented and stented devices is polyester (Figure

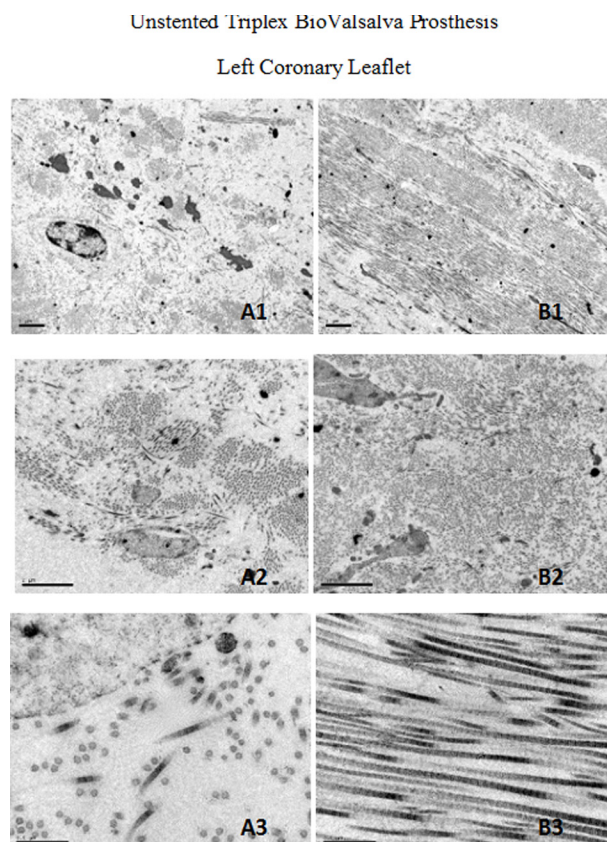Unstented Triplex BioValsalva Prosthesis

Left Coronary Leaflet

FIG. 19: Transmission electron microscopy of the left coronary leaflet of the unstented BioValsalva device. On the left is an area of scarce collagen content in the spongiosa. The cells are well preserved; no halo is visible either inside on in the vicinity. Some elastin fibers are noticeable. The collagen bundles are very loosely dispersed. Each filament is well individualized and a regular banding is suspected. Meanwhile, the collagen bundles of the ventricularis and the fibrosa lie as parallel assemblages of individual fibers. Each fiber shows a regular bonding characteristic.
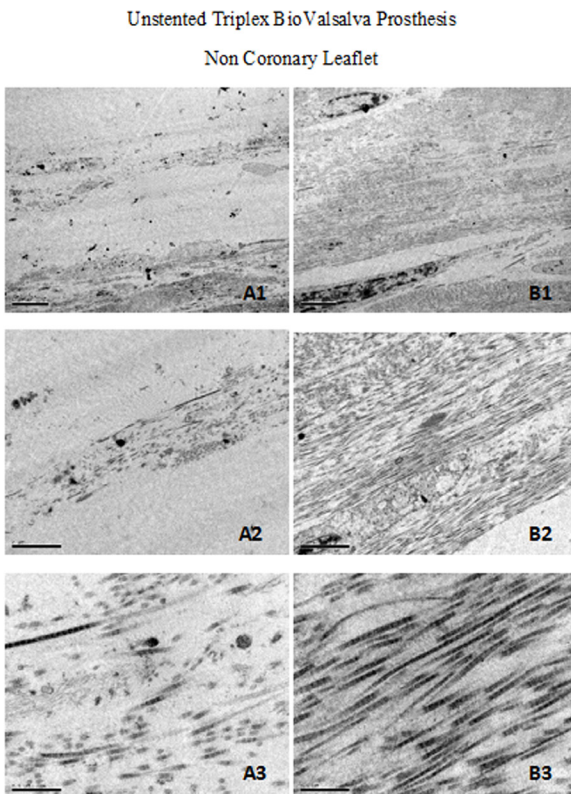
FIG. 20: Transmission electron microscopy of the non-coronary leaflet of the unstented BioValsalva device. The collagen content of the microphotographs of the left is highly dispersed in the spongiosa. The fibrils hold the regular banding characteristic of collagen. The elastin filaments are very scarce. The collagen bundles are abundant in the ventricularis and the fibrosa. The fibers are, individually and in parallel, assembled in bundles surrounding interstitial cells. The banding of the collagen filaments is perfectly regular and characteristic.

33b). The spectrum after cleaning was almost the same as those prior to cleaning, suggesting that no major surface chemical change occurred following cleaning (Figure 34b).

The surface chemistry measured with XPS differed from that measured with FTIR. While FRIP data support the PET fabric and SEPS sealing, XPS indicated oxygen (likely carbonyl groups)-rich sealing material and oxygen-poor fabric material. The known carbon-to-oxygen ratio in PET is 5:2, and SEPS does not contain any oxygen. Considering the significant difference in sampling depth between

XPS and FTIR (10 nm vs. higher than 10 microM), this discrepancy between XPS and FTIR may well reflect the fact that the surface of the sealed prostheses contains materials other than SEPS, and the "cleaned" surface was actually SEPS rather than PET. Therefore, after the cleaning procedure, the prosthesis was still covered by SEPS.

3. *Differential Scanning Calorimetry (DSC)*

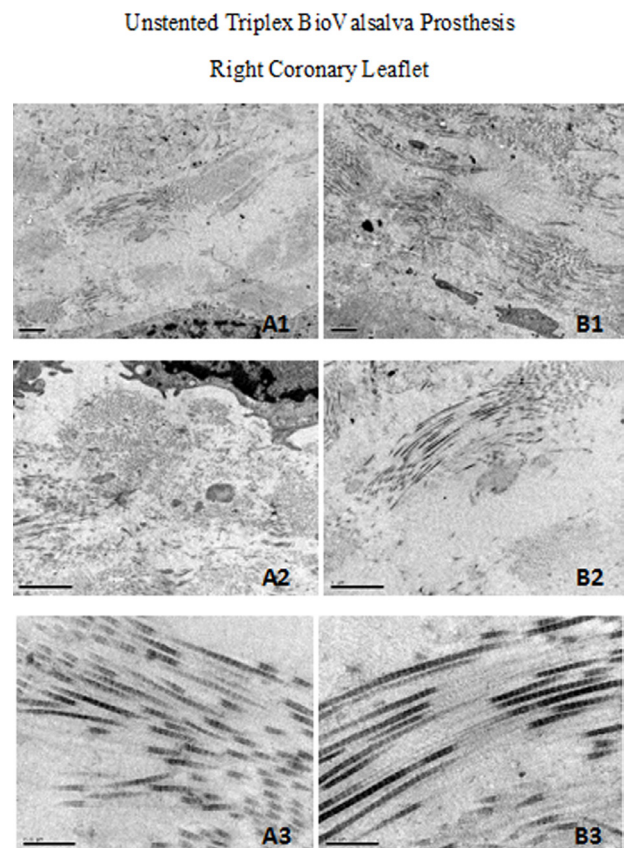Both unstented and stented devices displayed char-

FIG. 21: Transmission of the right coronary leaflet of the unstented BioValsalva device. The collagen content of the microphotographs of the left is poorly organized and highly dispersed. The ventricular interstitial cells are well preserved and the filaments of collagen hold the characteristic banding. The collagen content in the other layers, i.e., ventricularis and fibrosa, is more abundant, but the content of the collagen bundles was limited. The filaments are perfectly individualized, showing characteristic banding.

acteristics of polyester fiber (Table 4). The premelt onset temperature (~248°C), peak melting temperature (>250°C), premelt end temperature (~254°C), melt enthalpy (~50 J/g), and glass transition temperature Tg (~68°C) of unstented and stented devices were similar.

IV. DISCUSSION

The well-known Bentall operation has been accept-

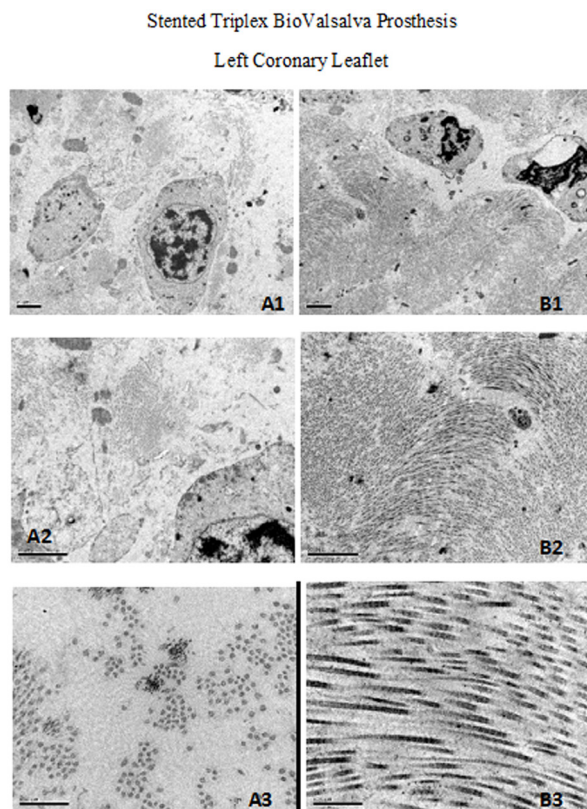Stented Triplex BioValsalva Prosthesis

Left Coronary Leaflet

FIG. 22: Transmission electron microcopy of the left coronary leaflet of the stented BioValsalva. The microphotographs of the left show a highly cellularized area in the spongiosa with dispersed filaments of collagen and rare elastin filaments. The cross-section of the poorly assembled bundles of collagen confirms that the individual filaments are perfectly individualized. In the areas of denser collagen of the ventricularis and the fibrosa, the cellularity is well preserved. The bundles of collagen that surround the interstitial cells show alternate longitudinal views and cross-sections, i.e., waviness. The filaments are perfectly individualized and show the regular pattern typical of collagen.
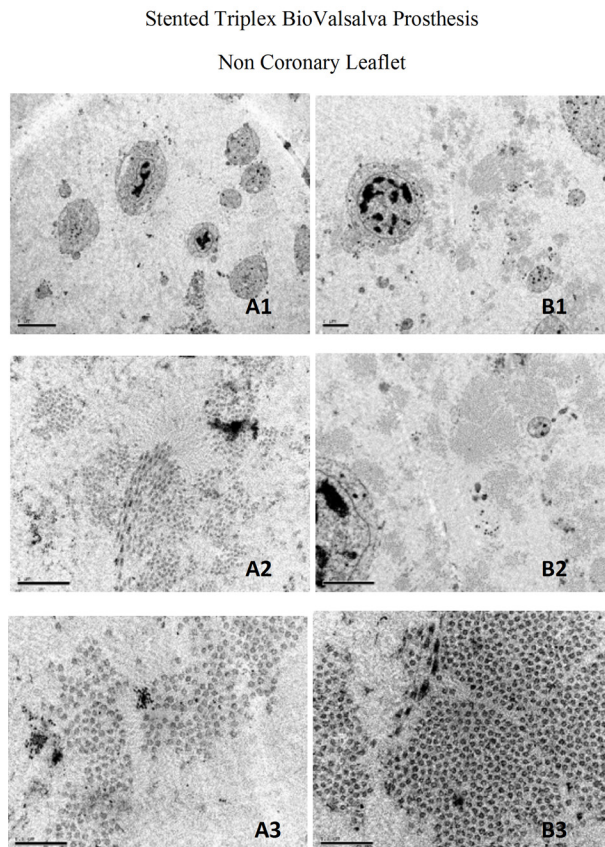
Stented Triplex BioValsalva Prosthesis

Non Coronary Leaflet

FIG. 23: Transmission electron microscopy of the non-coronary leaflet of the stented BioValsalva. The micrographs of the left show a highly cellularized content dispersed in the glucosaminoglycans in the spongiosa. The filaments of collagen are loosely assembled in bundles. Some scarce elastin filaments can be seen as well. The microphotographs of the right show a section with some interstitial cells surrounded by bundles of collagen filaments well individualized. Some scarce filaments of elastin are visible as well.

ed for several decades.[2,4,45] However, there is no real consensus regarding the technique that maximizes the long-term durability of this procedure.[46–48] In a nutshell, the technique can be valve sparing or can incorporate a valved conduit should the aortic valve need to be replaced.[49–52]

The BioValsalva prosthesis was designed to offer a valid option for elderly patients undergoing composite aortic root replacement incorporating the aortic valve and the aortic root itself; it closely matches the aortic root anatomy. This device has the capacity to reduce tension on the coronary arteries.[53]
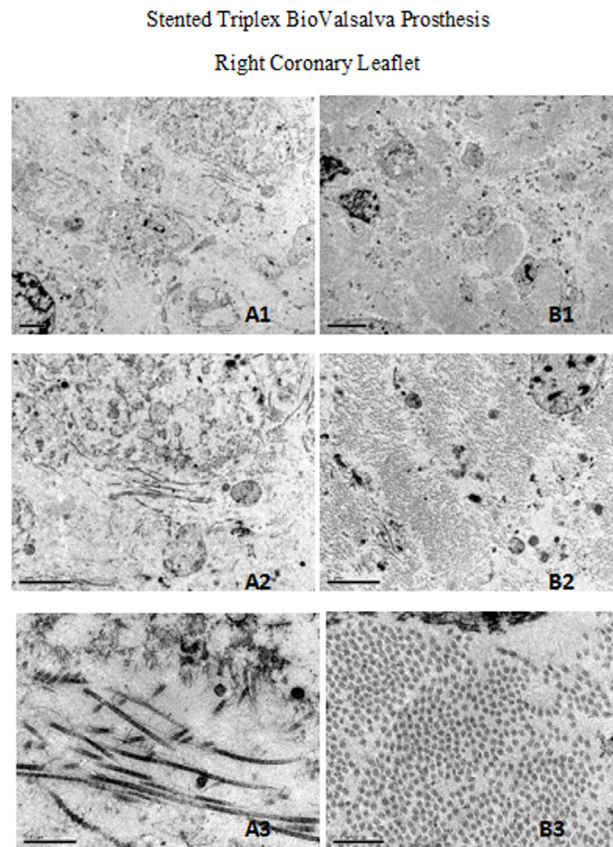
Stented Triplex BioValsalva Prosthesis

Right Coronary Leaflet

FIG. 24: Transmission electron microscopy of the right coronary leaflet of the stented BioValsalva. The micrographs of the left show a very limited collagen content in the spongiosa. There are numerous ventricular interstitial cells and dispersed filaments of elastin and collagen. The banding of the collagen filaments is perfectly regular. The microphotographs of the right show a dense assemblage of collagen bundles incorporating scarce elastin filaments and surrounding ventricular interstitial cells. The filaments of collagen were well individualized as seen in cross-section.

The concept of de Paulis is now widely accepted because it proved to be flexible. The pseudosinuses created by the skirt and the well-defined sinotubular junction facilitate near-normal valve function. The results achieved by De Paulis et al. have opened new avenues of treatment.[54–56]

This BioValsalva graft provides a more consistent and standardized approach to the Bentall procedure involving valve replacement. Surgeons now have a device that is directly available in the marketplace. It can be trimmed or amended by the surgeon according to the patient's anatomy. The need to undertake the sewing of various polyester tubes and/or fabric together with an aortic prosthetic valve has been eliminated. In other words, the potential shortcomings associated with the intraoperative construction of prosthesis have been considerably reduced.[57,58] The quality of the bench testings, the controls together with the requirements of the regulatory agencies (e.g., the FDA or the CFDA), offer additional guarantees.[59,60] Such a concept has been well accepted with bioprostheses. In addition, major manufacturers, such as St Jude Medical, OnX, and Sorin, manufacture valved conduits of the Gelweave Valslava graft fitted with their own me-
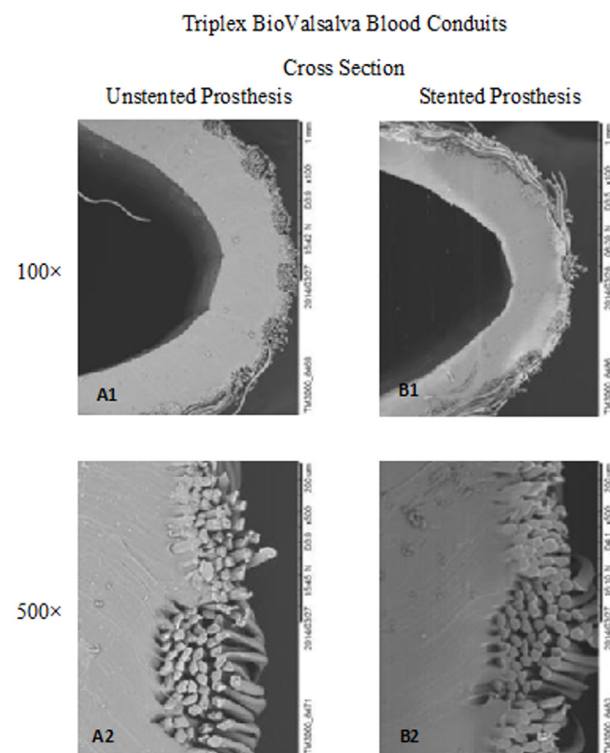
Triplex BioValsalva Blood Conduits

Cross Section

FIG. 25: SEM microphotographs of the cross-section of the BioValsalva devices. Both the unstented and the stented prostheses show a thin woven fabric (inside) to be exposed to the blood flow externally impregnated with a thermoplastic polymer, coated with a Teflon film (outside). The thermoplastic polymer is strongly anchored to the fabric and penetrates deeply in the wall of the polyester structure filling and the void spaces between the yarns.
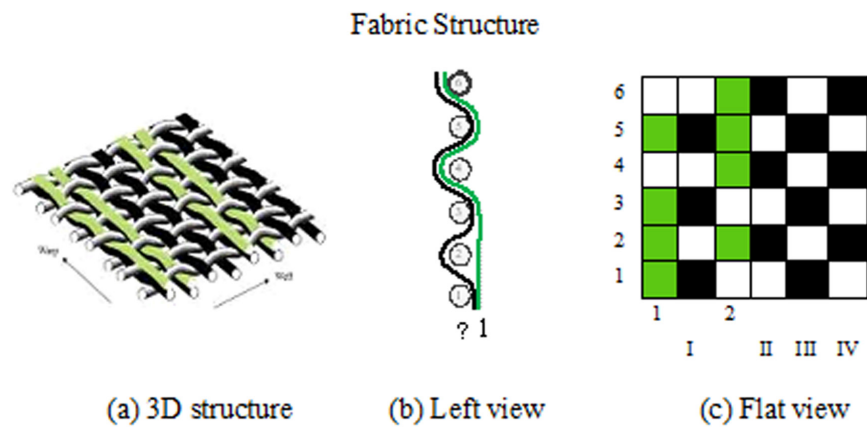
Fabric Structure

(a) 3D structure   (b) Left view   (c) Flat view

FIG. 26: The structure of the fabric is a ribbed-weave structure. It is a specially wave-backed weave consisting of two series of warp threads, face warp (green) and back warp (black), and one series of weft threads (white). The back warp interweaves with the wefts to form the back weave, which is 1-warp/1-weft, namely plain weave, while the face warps are over the plain weave, where every other two warps orm the face weave, which is 3-warp/1-weft, 1-warp/1-weft twill. The special warp-backed weave gives different surface aspects to the inside and outside of the fabric tube.
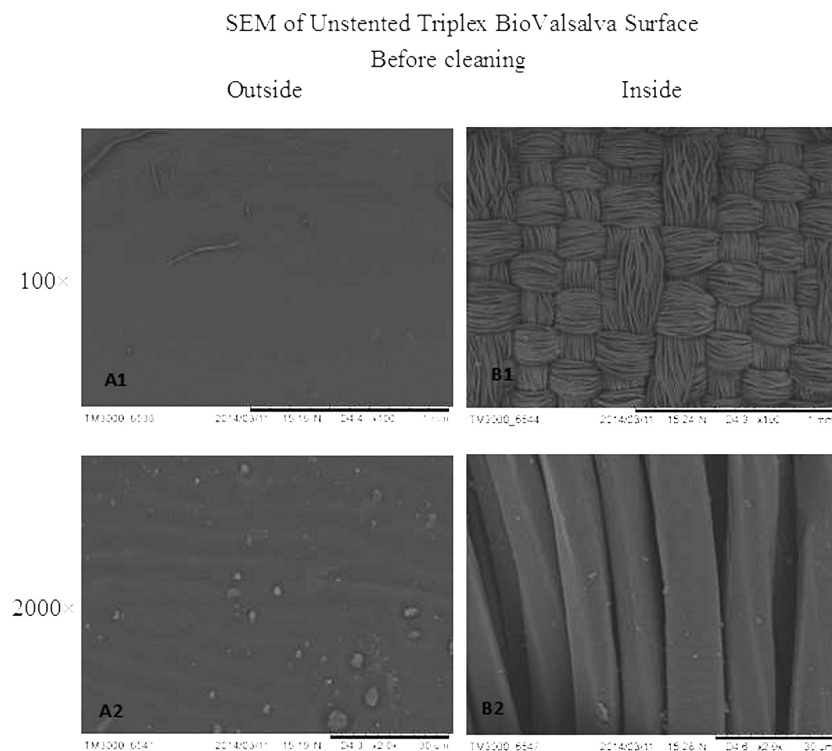
SEM of Unstented Triplex BioValsalva Surface

Before cleaning

Outside   Inside

FIG. 27: Scanning electron microscopy of the inside and the outside of the unstented Biovalsalva prosthesis. The external surface is smooth and glistening (A1:×100; A2:×2000). The structure of the polyester wave is clearly visible. This weave consists of two systems of warps (face wrap and back warp). In this face weave, the face warp is interlaced with the left in the ruler of 3/3 twill with an interval of two warps (B1: ×100; B2:×2000).

chanical valves that are commercially available.[61,62] The concept of valved Valsalva conduit has been well accepted after in-depth investigation[63–65]:

1. The surgical technique has been made easier and less time-consuming. The resulting blood conduits called Triplex maintain specific characteristics that are consistent between grafts. The addition of outer elastomeric layers makes the polyester impervious at implantation; thus, any bleeding is prevented.[66] The Triplex consist of three layers (inner polyester, central elastomer SEPS, and outer ePTFE wrap/film) and has been employed in thoracic surgeries, including the aortic arch.[67]

2. The construction of the polyester conduit is well designed for surgery. The prosthetic valve (stented or not) is ready for implantation. The skirt has a very attractive construction that mimics the Valsalva and allows the suturing of the coronary arteries with
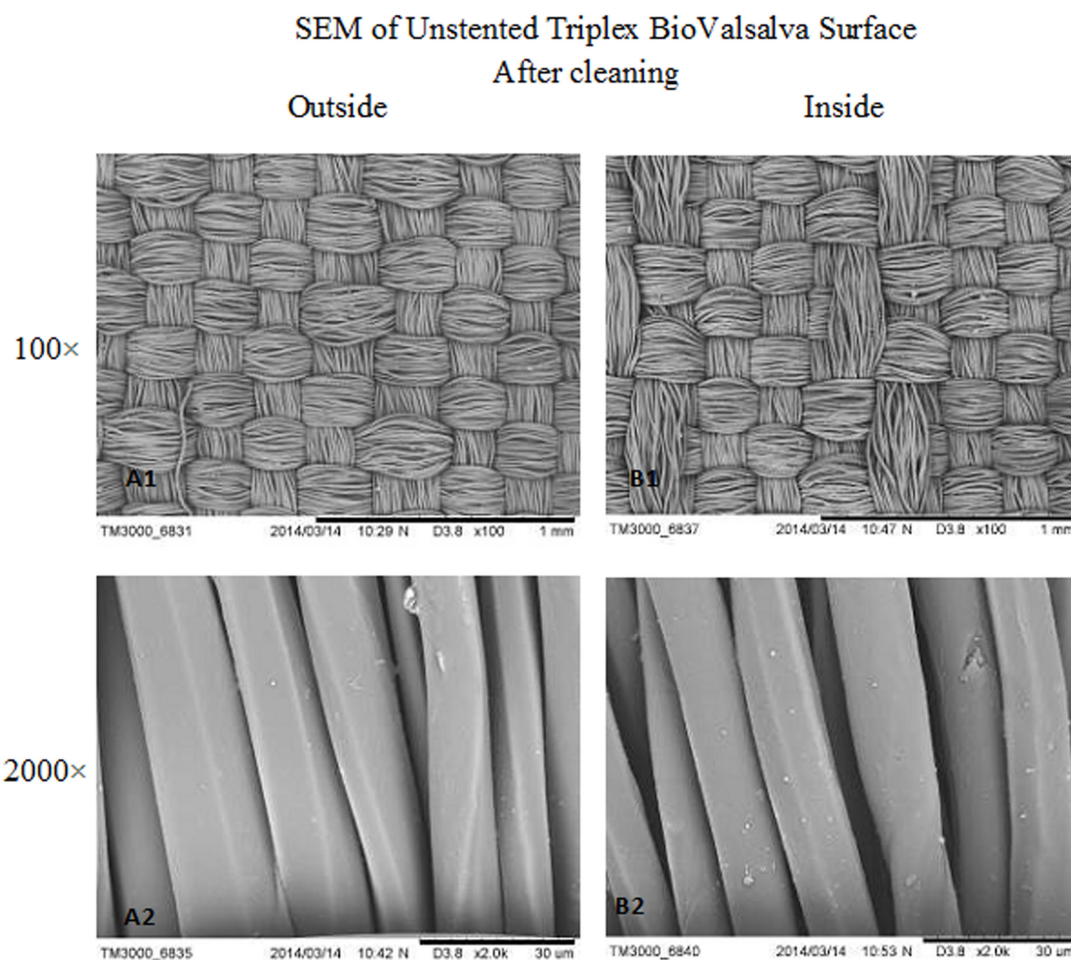

FIG. 28: Scanning electron microscopy of the inside and the outside of the unstented Biovalsalva prosthesis after cleaning. The side-by-side photos of the outside and the inside confirm that the weave of the polyester fabric (face warp and back warp) and one system of weft. The face weave is formed by interlacing face warp and weft. The back weave is formed by interlacing back warp and weft. The back weave is a traditional plain weave; in the face weave, the warp is interlaced with the weft in 3/3 twill with an interval of two warps.
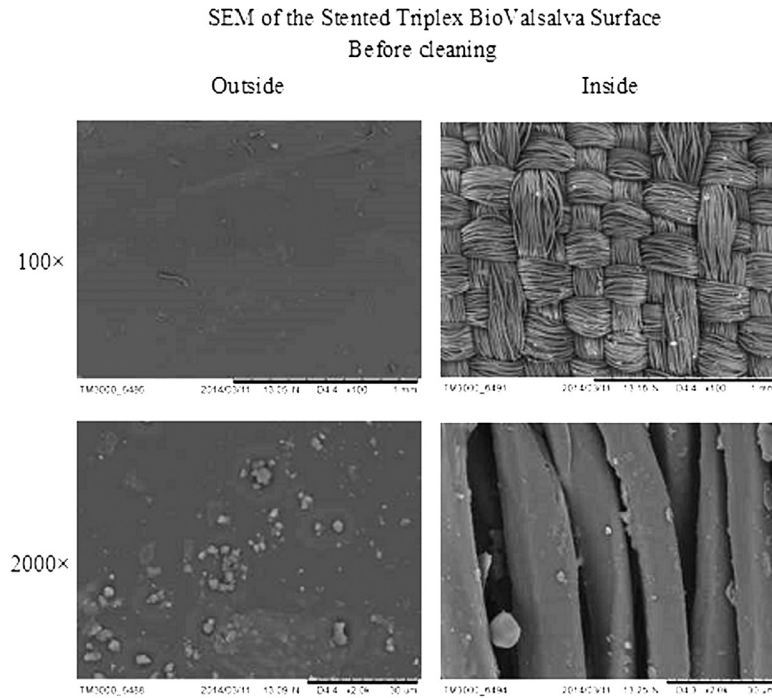
SEM of the Stented Triplex BioValsalva Surface
Before cleaning

Outside   Inside

FIG. 29: Scanning electron microscopy of the outside and inside the of the stented Biovalsalva prosthesis as received from the manufacture. Both the outside and the inside observation are similar to those of the unstented device.

SEM of Stented BioValsalva Surface
After cleaning

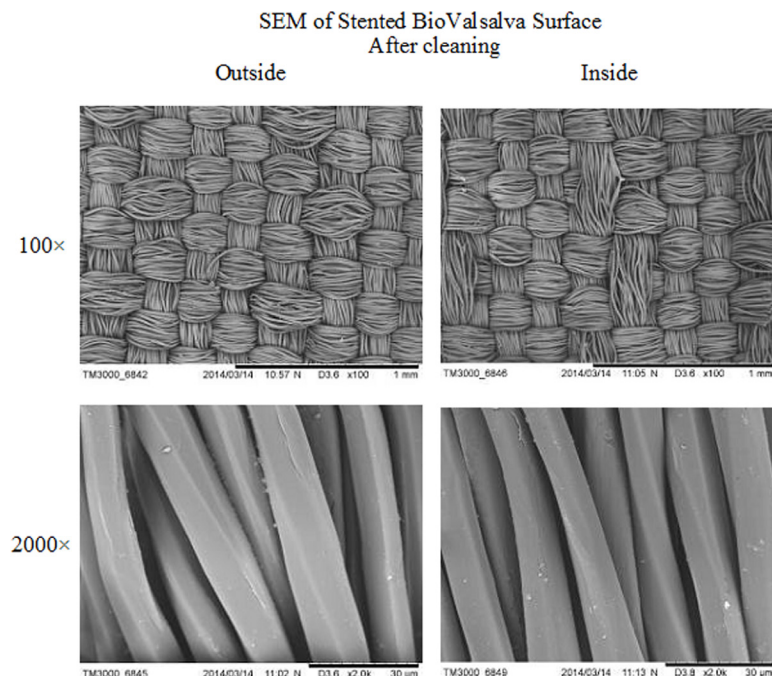Outside   Inside

FIG. 30: Scanning electron microscopy of the outside and inside of the stented Biovalsalva prosthesis after cleaning and eliminating the external coating. The structure of the polyester fabric was identical to the one observed in the unstented device.

TABLE 1: Fabric Features/Characteristics

	Fabric count (/mm)			Fabric structure	Thickness (mm)	Mass (g/cm²)	Porosity (%)
	Upper Warp	Inner Warp	Weft				
Unstented	4.27±0.09 8.18	3.91±0.11	5.44±0.10	Warp rib weave*	0.272±0.004	0.0124±0.0003	66.963
Stented	4.20±0.06 8.05	3.85±0.09	5.48±0.04	Warp rib weave*	0.271±0.003	0.0123±0.0002	67.166

*Note: All the data come from the fabric of the body after cleaning.

TABLE 2: Yarn and Filament Features of Fabric

		Unstented			Stented		
		Upper Warp	Inner Warp	Weft	Upper Warp	Inner Warp	Weft
No. of filaments in each yarn		54	54	27×2	54	54	27×2
Yarn linear density* (dtex)		110.44	109.00	106.46	108.68	111.73	108.04
Filament diameter (um)		13.74±0.60	13.65±0.55	13.49±0.45	13.63±0.55	13.82±0.55	13.59±0.64
Filament linear density* (dtex)		2.05	2.02	1.97	2.01	2.07	2.00
Filament tensile elongation(%)		32.56±2.30	30.49±2.75	31.72±2.11	33.10±2.99	31.23±2.71	35.23±2.16
Filament tensile breakage force(cN)		7.38±0.36	7.23±0.34	7.37±0.36	7.34±0.39	7.44±0.33	7.46±0.38
Filament tensile breakage strength	(cN/dtex)	3.60±0.18	3.58±0.17	3.74±0.18	3.65±0.20	3.59±0.16	3.73±0.19
	(Mpa)*	497.15	494.04	516.53	503.70	495.83	514.60
Filament modulus of elasticity	(cN/dtex)	13.55±0.55	14.22±1.10	14.81±1.56	13.51±0.96	13.47±1.24	13.54±0.84
	(Mpa)*	1870.52	1961.88	2043.71	1863.90	1859.07	1867.83

*Note: All the data were obtained from the fabric of the body after cleaning. The yarn linear density and the filament linear density were both calculated according to the measured diameter of the filament. The values of filament tensile breakage strength and filament modulus of elasticity in Mpa were both converted from the unit in cN/dtex.

considerably reduced tensions. The body, with its crimps perpendicular to the blood flow, can be tailored according to the requirements of the anatomy of the patients.[68–70]

3. The polyester fabrics selected to manufacture the BioValsalva appear to be well adapted for this procedure. They are made totally impervious by the application of a thermoplastic elastomer and an outer PTFE wrap/film that is thermally bonded. This kind of fabric is strong enough to resist long-term dilatation and/or degradation. Its use in open vascular surgery has not been associated with device-related adverse events.[37,71]

4. Chemically processed porcine valves have been implanted for 50 years and

are acknowledged as a satisfactory device. The selection of a porcine valve to manufacture the Triplex Biovalsalva prosthesis makes sense. Porcine tissue is less structurally homogeneous than bovine tissue with respect to collagen and fiber tissue orientation.[72,73] The porcine valve leaflet does contain a spongiosa layer. This spongiosa accumulates large amounts of hydrated proteoglycans and/or polysaccharides that reduce friction between the ventricularis and the fibrosa. The spongiosa is loose and watery and is of varying thickness; it forms the core of the cusp near the base, proximal to the aortic wall. The spongiosa consists of radially oriented collagen fibers and cells scarcely disperse. It is proximately absent near the free edge. The spongiosa
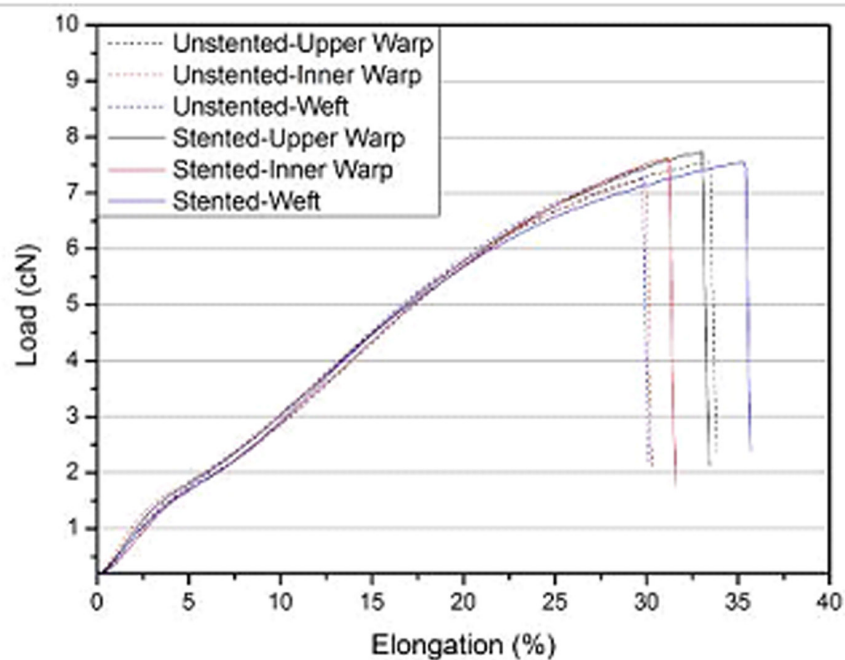

FIG. 31: Load elongation curve of the filaments. For each kind of yarn (upper warp, inner warp and weft, both on unstented and stented devices), 20 filaments were chosen randomly from 10 different yarns for the filament tensile test. The data presented in the table are the mean value of the 20 times tests.

TABLE 3: Surface Elemental Composition Measured with XPS

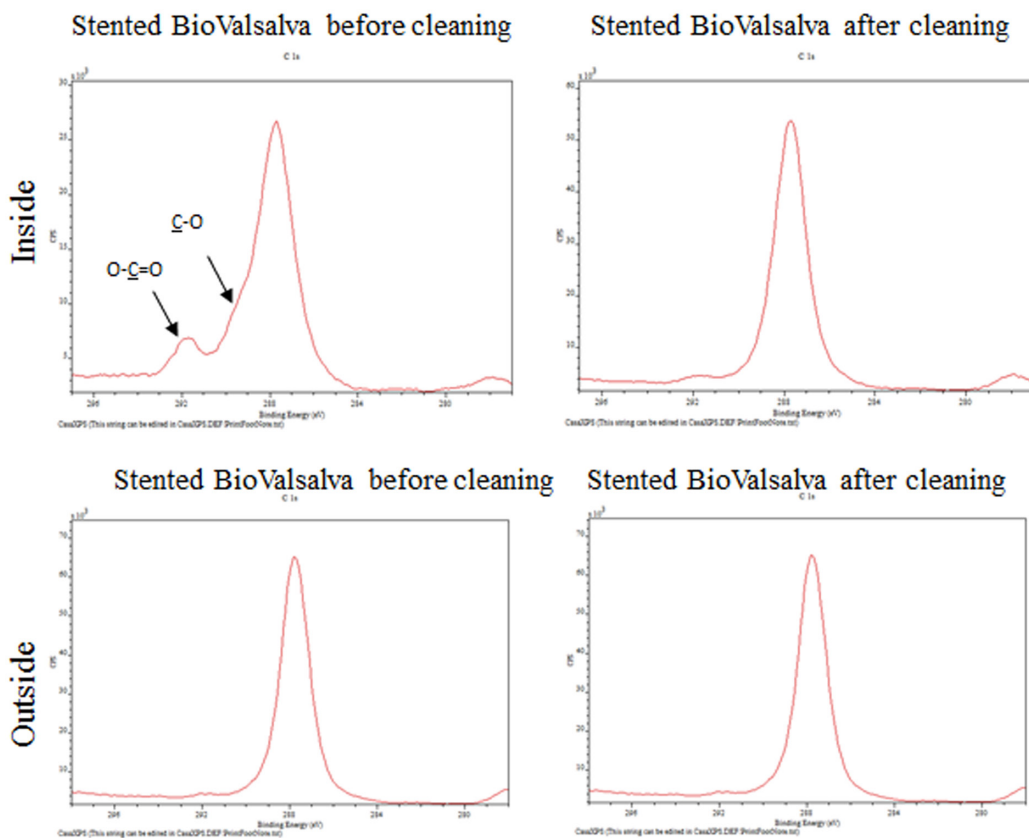| BioValslava	Elemental Composition (%)						
	C	O	N	Ca	Na	Zn	Si
Side A							
Before cleaning	67.5	25.3	0.5	0.2	0.1	0.4	6.0
After cleaning	87.2	9.3	0.3	0.2	0.2	1.1	1.7
Side B							
Before cleaning	88.6	8.3	0.3	0.2	0.1	0.3	2.1
After cleaning	88.7	8.1	0.4	0.2	0.2	0.4	2.0

FIG. 32: High-resolution C_{1s} spectra of the BioValsava prostheses measured with XPS, showing the distinct presence of oxygen moieties inside the non-cleaned fabrics, and the similar spectra after cleaning.

gives the cusp of the leaflet its deformability and allows the collagen and the elastin fibers to easily slide over each other during the cardiac cycle. The fibrosa also dampen the vibrations in the fibrosa associated with leaflet deformation during diastole. The valvular interstitial cells are dispersed in the three layers of the leaflets. They primarily contribute to maintain the structural integrity of the leaflet tissue. These valvular interstitial cells have the characteristics of both fibroblasts and smooth muscle cells. However, they do not survive to the chemical processing of the tissues.[74]

The chemical processing of the porcine aortic valve results in the cross linking of proteins, especially collagen. The glutaraldehyde proved to be the most efficient; it inhibits autolysis, enhances the me-

chanical stability, and creates the possibility of having valves available from the shelf. Other chemicals, such as formalin, epoxy, and carbodiimide, are now history. The fixation locks the structure at one phase of the cardiac cycle.[75] It is accompanied by the loss of endothelium, interstitial cell viability, and collagen bundles. Therefore, as a result of the chemical processing of the tissues, the porcine aortic valve totally loses its viability. It is misappropriately identified as a bioprosthesis. Based upon the practice of the last several decades, this product cannot be challenged. However, it is a singular material, and the quality of this material depends upon the conditions of processing. These valves differ in many respects from native valves, for example, in their opening and closing.

Stented porcine valves are made from a single pig valve sewn onto a plastic stent whose bone is reinforced with a metal ring. The stent and the ring are covered with a polyester cloth. Unstented porcine
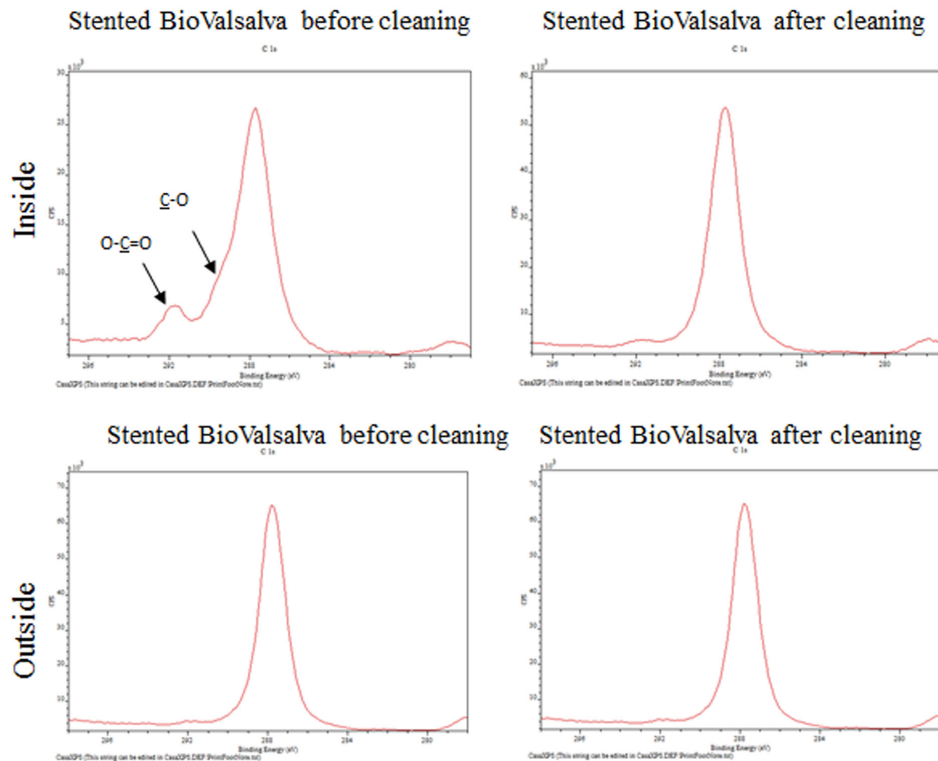

FIG. 33: FTIR of the outside and the inside of the blood conduit of the BioValsalva prosthesis as received.

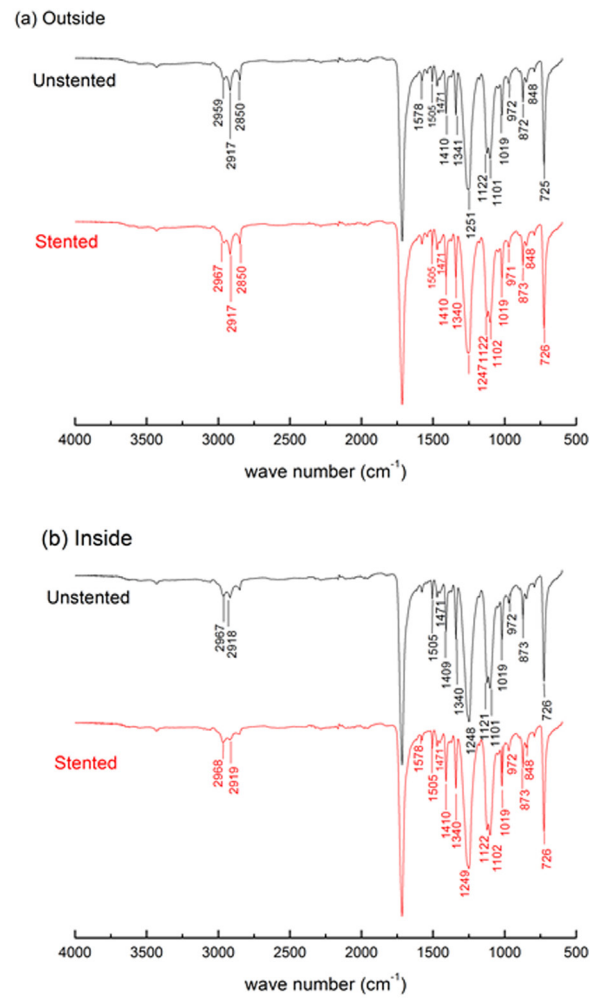FTIR of the Blood Conduits (after elimination of the coating)

FIG. 34: FTIR of the outside and the inside of the blood conduit of the BioValsalva prosthesis after digestion of the coating.

TABLE 4: Differential Scanning Calorimetry

	Premelt Onset Temperature (°C)	Peak Melting Temperature (°C)	Premelt End Temperature (°C)	Melt Enthalpy (J/g)	Tg (°C)
Unstented	248.2	251.4	254.1	50.9	73.0
Stented	247.4	250.4	249.1	49.8	68.0

*Note: All the data come from the fabric of the body after cleaning.

valves are also made from a single pig valve by removing the entire aortic root and adjacent aorta.[32–37] They are scalloped before they are sutured to the Triplex tube.[39,40] There is no real benefit to use the leaflet of different aortic valves as in the Hancock MO bioprosthesis.[76] This concept was based on the stiffness of the septal leaflet. Despite differences in the size and morphology of the leaflets, selecting valves from a single pig appears to be the most appropriate approach.

The right coronary leaflet is the longest and the non-coronary the smallest. The manufacture of the bioprosthesis follows a very careful examination of the aortic valve with naked eye. Practically every leaflet can be divided into several areas. The appositional area is the strip where the leaflets touch one another. The non-appositional area is the strip where the leaflet is anchored to the aortic wall. This non-commissural area does not touch the other two leaflets; it is the pressure bearing surface. The leaflet flexion area is the curvature of the leaflet observed in the region of transition between the appositional and non-appositional parts.[77]

The inflow surface is always rougher, with a complete loss of endothelial cells. The outflow surface made of the subendothelial layer is smoother but is devoid of endothelial cells that are destroyed during the tissue processing. Every valve consists of three main sections that can be considered in parallel: ventricularis, spongiosa, and fibrosa from the inflow to the outflow. The interstitial cells do not retain their viability during chemical processing.

Some authors recommend the decellularization of the leaflet to remove the major cellular immunological components.[78] However, *in vivo,* such a treatment does not present any evident advantage.[79] In the valves hereby selected, high celluarity was well evidenced, scarce elastic fibers were visible, and collagen was always present with various orientations. Inflammatory cells were present as well. The strict rules of the fixation procedure guarantee the durability of the valve, whereas decellularization treatment causes major alterations to the biological structures.[81–84]

Thus, the BioValsalva conduit fulfills the 3Bs: biocompatibility, biofunctionality, and biodurability. It provides important benefits for the Bentall procedure.[42]

The additional anticipated benefits of the BioValsalva devices compared to the Valsalva fitted with a mechanical valve consist in the absence of mandatory administration of long-term blood thinners to the patients. This is particularly important in elderly patients or in countries where anticoagulants are very expensive. However, the valved conduits hosting a mechanical valve offer the advantage of durability. Whereas the Gelweave Valsalva is stored dry and might theoretically become a biosynthetic conduit after the gelatin is digested, the Triplex BioValsalva prosthesis is preserved in a solution of low-concentration glutaraldehyde because of the porcine bioprosthesis. This concept makes the wall of the blood conduit stiffer, and the *in vivo* degradability of the seal has not yet been documented. Harvesting devices at autopsy and/or reoperation will allow us to investigate the fate of this polymer coating. The Triplex BioValsalva prosthesis, because of the storage in a solution of glutaraldehyde, must be abundantly rinsed prior to implantation.

V. CONCLUSION

Triplex BioValsalva grafts offer an avenue to better reconstruct the anatomy of the aortic root with respect to the 3Bs: biofunctionality, biodurability, and biocompatibility. The unique features of these prostheses are (1) a short section of polyester woven with a belly shape parallel to the blood flow, (2) the shape of the skirt in which length is equal to the aorta diameter with some capacity to expand its diameter after pressurization, and (3) the generation of pseudo-sinuses of Valsalva. It is sutured to the body a polyester tube whose crimps are perpendicular to the blood flow that can be tailored by the surgeon at implantation. However, the Bentall procedure remains a challenge, and adverse events cannot be fully eliminated. Overall, this device can contribute to the prevention of device-related adverse events.

ACKNOWLEDGMENTS

REFERENCES

1. Bentall H, De Bono A. A technique for complete replacement of the ascending aorta. Thorax.1968;23:338–9.

2. Etz CD, Bischoff MS, Bodian C, Roder F, Brenner R, Griepp RB, Di Luozzo G. The Bentall procedure: Is it the gold standard? A series of 597 consecutive cases. J Thorac Cardiovasc Surg. 2010;140:S64–S70.

3. Lusini M, Pollari F, Chello M, Covino E. Right coronary ostial aneurysm following a Bentall procedure. J Card Surg. 2011;26:632–3.

4. Galicia-Tornell MM, Marín-Solís B, Fuentes-Orozco C, Martínez-Martínez M, Villalpando-Mendoza E, Ramírez-Orozco F. The Bentall procedure in ascending aortic aneurysm: hospital mortality. Cir Ciruj. 2010;78:45–5.

5. Etz CD, Homann TM, Silovitz D, Spielvogel D, Bodian CA, Luehr M, DiLuozzo G, Plestis KA, Griepp RB. Long-term survival after the Bentall procedure in 206 patients with bicuspid aortic valve. Ann Thorac Surg. 2007;84:1186–94.

6. David TE, Feindel CM. An aortic valve-sparing operation for patients with aortic incompetence and aneurysm of the ascending aorta. J Thorac Cardiovasc Surg. 1992;103:617–22.

7. David TE, Ivanov J, Armstrong S, Feindel CM, Webb GD. Aortic valve-sparing operations in patients with aneurysms of the aortic root or ascending aorta. Ann Thorac Surg. 2002;74:S1758–S1761.

8. Kouchoukos NT, Wareing TH, Murphy SF, Perrillo JB. Sixteen year experience with aortic root replacement- Results of 172 operations. Ann Surg. 1991;214:308–18.

9. Michielon G, Salvador L, Da Col U, Valfre C. Modified Button Bentall operation for aortic root replacement: the miniskirt technique. Ann Thorac Surg. 2001;72:S1059–S1064.

10. Albertini A, Dell'Amore A, Zussa C, Lamarra M. Modified Bentall operation: the double sewing ring technique. Eur J Cardio-Thorac Surg. 2007;32:804–6.

11. Christenson JT, Sierra J, Trindade PT, Didier D, Kalangos A. Bentall procedure using cryopreserved valved aortic homografts: mid to long-term results. Tex Heart Inst J. 2004;31:387–91.

12. Choudhary SK, Talwar S, Kumar AS. Bentall operation with valved homograft conduit. Tex Heart Inst J. 2000;27:366–8.

13. Vuran C, Simon P, Wollenek G, Özker E, Aslim E. Midterm results of aortic valve replacement with cryopreserved homografts. Balkan Med J. 2012;29:170–3.

14. Stewart AS, Takayama H, Smith CR. Modified operation with a novel biologic conduit. Ann Thorac Surg. 2010;89:938–41.

15. Galiñanes M, Meduoye A, Ferreira I, Sosnowski A. Totally biological composite aortic stentless valved conduit for aortic root replacement: 10-year experience. J Cardiothor Surg. 2011;6:86–95.

16. Tabata M, Takayama H, Bowdish ME, Smith CR, Stewart AS. Modified Bentall operation with bioprosthetic valved conduit: Columbia University experience. Ann Thorac Surg. 2009;87:1969–70.

17. Vrandecic M, Gontijo Filho B, Fantini F, Barbosa J, Martins I, de Oliveira OC, Martins C, Max R, Drumond L, Oliveira C, Ferrufino A, Alcocer E, Silva JA, Vrandecic E. Use of bovine pericardial tissue for aortic valve and aortic root replacement: long-term results. J Heart Valve Dis. 1998;7:195–201.

18. Westaby S, Katsumata T, Vaccari G. Coronary reimplantation in aortic root replacement: a method to avoid tension. Ann Thorac Surg. 1999;67:1176–7.

19. Maselli D, Guarracino F, Bajona P, Bellieni L, Minzioni G. Adjustable sinotubular junction for aortic valve reimplantation procedures. Ann Thorac Surg. 2007;83:700–2.

20. Demers P, Miller DC. Simple modification of "T. David-V" valve-sparing aortic root replacement to create graft pseudosinuses. Ann Thorac Surg. 2004;78:1479–81.

21. Maureira P, Vanhuyse F, Martin C, Lekehal M, Carteaux J-P, Tran N, Villemot J-P. Modified Bentall procedure using two short grafts for coronary reimplantation: long-term results. Ann Thorac Surg. 2012;93:443–9.

22. Cabrol C, Pavie A, Gandjbakhch I. Complete replacement of the ascending aorta with reimplantation of the coronary arteries. New surgical approach. J Thorac Cardiovasc Surg. 1981;81:309–15.

23. Krasopoulos G, David TE, Armstrong S. Custom-tailored valved conduit for complex aortic root disease. J Thorac Cardiovasc Surg. 2008;135:3–7.

24. Svensson LG. Sizing for modified David's reimplantation procedure. Ann Thorac Surg. 2003;76:1751–3.

25. Urbanski PP, Frank S. New vascular graft for simplification of the aortic valve reimplantation technique. Interact Cardiovasc Thorac Surg. 2008;7:552–4.

26. Neveux JY, Dervanian P, Folliguet TA, Mace L, Guluta V. Technical modification for anastomosis of low-lying coronary ostia in Bentall procedure. Ann Thorac Surg. 1993;56:383–4.

27. Kalkat MS, Edwards MB, Taylor KM, Bonser RS. Composite aortic valve graft replacement, mortality outcomes in a national registry. Circulation. 2007;116(Suppl I):I301–

I306.

28. Albes, JM, Stock, UA, Hartrumpf M. Restitution of the aortic valve: what is new, what is proven, and what is obsolete? Ann Thorac Surg. 2005;80:1540–9.

29. Inaba H, Kaneko T, Ezure M, Sato Y, Hasegawa Y, Shibasaki I. Aortic root replacement with a mechanical valve and prosthetic conduit for the complicated degeneration of the ascending aorta resulting from infective endocarditis. Ann Thorac Cardiovasc Surg. 2007;13:355–89.

30. De Paulis R, Nardi P, De Matteis GM, Polisca P, Chiariello L. Bentall procedure with a stentless valve and a new aortic root prosthesis. Ann Thorac Surg. 2001;71:1375–6.

31. De Paulis R, De Matteis GM, Nard P, Scoffa R, Colella DF, Bassano C, Tmai F, Chiariello L, One year appraisal of a new aortic root conduit with sinuses of valsalva. J Thorac Cardiovasc Surg. 2002;123:33–9.

32. De Paulis R, Scaffa R, Forlais S, Chiarello L. The Valsalva graft in aortic valve repair and replacement. MMCTS 2005;1129. (doi 10. 1510/mmcts.2004.000992)

33. De Paulis R, De Matteis GM, Nardi P, Scaffa R, Colella DF, Chiariello L. Research methods and new therapies: a new aortic Dacron conduit for surgical treatment of aortic root pathology. Ital Heart J. 2000;1:457–63.

34. Lee S, Lee LH, Choi KY, Rhee JM. Glass transition behavior of polypropylene/polystyrene/styrene-ethylene-polypropylene block copolymer blends. Polymer Bull. 1998;40:765–71.

35. Morota T, Takamoto S. Development and physical characteristics of novel zero-porosity vascular graft Triplex. Ann Vasc Dis. 2013;6:67–73.

36. Planthottam S, Roman R, Landers J, Mann RH, Joseph K, Ugolick R. Styrene ethylene-butylene and ethylene- propylene block copolymer hot melt pressure sensitive adhesives. United States Patent 5,618,883 April 8, 1997.

37. Fu Y, Guidoin R, De Paulis R, Lin J, Li B, Wang L, Qin B, Desaulniers D, Nutley M, Zhang Z. The Gelwave Valsalva graft to better reconstruct for anatomy of the aortic root. J Long-Term Eff Med Implan. In press.

38. Ukpabi P, Marois Y, King M. Deng X, Martin L, Laroche G, Douville Y, Guidoin R. The Gelweave polyester arterial prosthesis. Can J Surg. 1995;38:322–31.

39. Berg GA, Sonecki P, Borg RBS, MacArthur KJD. The Vascutek Elan porcine prosthesis. The Glasgow experience. In: Aortic Root Surgery. CA Yankah, Y Wang, R Hertzer, Eds. New York: Springer Verlag; 2010. Pp. 369–405.

40. Flynn M, Iaccovoni A, Pathi V, Butler J, MacArthur KJD, Berg GA. The aortic Elan Stentless aortic valve: excellent hemodynamics and ease of implantation. Semin Thorac Cardiovasc Surg. 2001;13:48–54.

41. International Standards Organization. Cardiovascular implants-Tubular vascular prostheses. ISO 7198. 1998.

42. Xu Z, Fan Y, Geelkerken RM, Deng X, King M, Traore A., Ingle N, Turgeon S, McGregor R, Dionne G, Zhang Z, Marinov GR, Legrand AP, Guzman R, Zhang H, Yin T, Douville Y, Nutley M, Renou JP. Guidoin R. Characterization

43. King MW, Guidoin R, Gunasekera K, Martin L, Marois M, Blais P, Maarek JM, Gosselin C. An evaluation of Czechoslovakian polyester arterial prostheses. ASAIO J. 1984;7:114–33.

44. Guidoin RG, King M, Marois M, Martin L, Marceau D, Hood R, Maini R. New polyester arterial prostheses from Great Britain: an *in vitro* and *in vivo* evaluation. Ann Biomed Eng. 1986;14:351–67.

45. Hagl C, Strauch JT, Spielvogel D, Galla JD, Lansman SL, Squitieri R, Bodian CA, Griepp RB. Is the Bentall procedure for ascending aorta or aortic valve replacement the best approach for long-term event-free survival? Ann Thorac Surg. 2003;76:698–703.

46. Joo HC, Chang BC, Youn YN, Yoo KJ, Lee S. Clinical Experience with the Bentall Procedure: 28 Years. Yonsei Med J. 2012;53:915–23.

47. Etz CD, Girrbach FF, Von Aspern K, Battellini R, Dohmen P, Hoyer A, Luehr M, Mohr FW. Longevity after aortic root replacement: Is the mechanically valved conduit really the gold standard for quinquagenarians? Circulation. 2013;128(Suppl1): S253–S262.

48. Mazzola A, Gregorini R, Villani C, Giancola R. A simple method to adapt the height of the sinotubular junction of the de Paulis Valsalva graft to the height of the patient's sinuses in David reimplantation procedure. Eur J Cardiothorac Surg. 2005;27:925–6.

49. Welbert L, De Paulis R, Scoffa R, Maselli D, Bellisario A, Dallessandro S. Re-creation of a sinus like graft expansion in Bentall procedure reduces stress at the coronary button anastomoses: a finite element study. J Thorac Cardiovasc Surg. 2009;137:1082–7.

50. Inamura S, Furuya H, Yagi K, Ikeya E, Yamaguchi M, Fujimura T, Kanabuchi K. Aortic root reconstruction in two patients with chronic aortic dissection by aortic valve-sparing. Procedures using a new aortic root conduit with the sinuses of Valsalva (De Paulis Valsalva graft). Tokai J Exp Clin Med. 2006;31:83–6.

51. Patel ND, Williams JA, Barreiro CJ, Bethea BT, Fitton TP, Dietz HC, Lima JAC, Spevak PJ, Gott VL, Vricella LA, Cameron DE. Valve-sparing aortic root replacement: early experience with the De Paulis Valsalva graft in 51 patients. Ann Thorac Surg. 2006;82:548–53.

52. De Paulis, R, De Matteis GM, Nardi P, Scaffa R, Buratta MM, Chiariello L. Opening and closing characteristics of the aortic valve after valve-sparing procedures using a new aortic root conduit. Ann Thorac Surg. 2001;72:487–94.

53. De Paulis R, Tomai F, Bertoldo F, Ghini AS, Scoffa R, Nardi P, Chiariello L. Coronary flow characteristics after a Bentall procedure with or without sinuses of Valsalva. Eur J Cardiothorac Surg. 2004;26:66–72.

54. Maselli D, Welbert L, Scoffa R. De Paulis R. How to

achieve an aortic root remodelling by performing an aortic root reimplantation. Eur J Cardiothorac Surg. 2012;42:e136–e137.

55. Maselli D, Minzioni G. A technique to reposition sinotu-bular junction in aortic valve reimplantation procedures with the de Paulis Valsalva graft. Eur J Cardiothac Surg. 2006;29:107–109.

56. Maselli D, De Paulis R, Scaffa R, Weltert L, Bellisario A, Salica A, Ricci A. Sinotubular junction size affects aortic root geometry and aortic valve function in the aortic valve reimplantation procedure: an in vitro study using the Val-salva graft. Ann Thorac Surg. 2007;84:1214–18.

57. Bochenek-Klimczyk K, Lau KKW, Galiñanes M, Sos-nowski AW. Preassembled stentless valved-conduit for the replacement of the ascending aorta and ascending root. In-teract Cardiovasc Thorac Surg. 2008;7:964–8.

58. Tannera A, Yamaguchi A. Yurik, Nogachi K, Naeto K, Na-gano H, Takahashi M, Adochi H. Clinical experience with a new vascular graft free from biodegradable material In-teract. Cardiovasc Thorac Surg. 2011;12:758–61.

59. Dhruva SS, Bero LA, Redberg RF. Strength of study evi-dence examined by the FDA in premarket approval of car-diovascular devices. J Am Med Assoc. 2209;302:2679–85.

60. O'Connor AB. The need to improved access to FDA re-views. J Am Med Assoc. 2009;302:191–3.

61. Vanney GP, Brendzel AM, Ringdal JR, inventors; St. Jude Medical, Inc., assignee. Prosthetic heart valve with in-creased valve lumen. United States Patent US 6007577. 1999 Dec 28.

62. Bokros JC, Stupka JC, More RB, inventors; Medical Car-bon Research Institute, Llc. assignee. Prosthetic heart valve. United States Patent US 6096075 A. 2000 Aug 1.

63. .De Paulis R. Prosthetic tubular aortic conduit and meth-od for manufacturing the same. US 6352554 B2. June 14, 2007.

64. De Paulis R, Schmitz C, Scoffa R, Nardi P, Chiariello L, Reul H. *In-vitro* evaluation of aortic valve prosthesis in a novel valved conduit with pseudosinuses of Valsalva. J Thorac Cardiovasc Surg, 2005;130:1016–21.

65. De Paulis R, De Matteis GM, Nardi P, Scaffa R, Bassano C, Chiariello L. Analysis of valve motion after the reim-plantation type of valve-sparing procedure (David I) with a new aortic root conduit. Ann Thorac Surg. 2002;74:53–7.

66. Okata T, Veda H, Kobayaski K, Fukuda H, Miyamoto Y. Terumo-Triplex grafts for total arch replacement: analy-sis of post-operative graft performance. J Artif Organs. 2012;15:240–3.

67. De Paulis R, Scaffa R, Maselli D, Salica A, Bellisario A, Weltert L. A third generation of ascending aorta da-cron graft: preliminary experience. Ann Thorac Surg. 2008;85:305–9.

68. Guidoin R, Marceau D, Couture J, Rao TJ, Merhi Y, Roy PE, DelaFaye D. Collagen coatings as biological sealants for tex-tile arterial prostheses. Biomaterials. 1989;10:156–65.

69. Marois M. Chakfe N, Guidoin R, Duhamel RC, Roy R, Marois M, King MW, Douville Y. An albumin-coated poly-ester arterial graft: in vivo assessment of biocompatibility and healing characteristics. Biomaterials. 1996;17:3–14.

70. Bordenave L, Caix J, Basse-Cathalinat B, Baquey C, Midy D, Baste JC, Constans H. Experimental evaluation of a gelatin-coated polyester graft used as an arterial substitute Biomaterials. 1989;10:235–42.

71. Etz CD, Homann T, Silovitz D, Bodian CA, Luchr M, Di-luozzo, Plestis KS, Griepp RB. Vascular graft replacement of the ascending and descending aorta: do Dacron grafts grow? Ann Thorac Surg. 2007;84:1206–12.

72. Schoen FJ, Levy RJ. Tissue heart valves: current challeng-es and future research perspectives. J Biomed Mater Res. 1999;47:439–65.

73. Misfeld M, Sievers HH. Heart Valve macro and micro-structures. Phil Trans R Soc B. 2007;362:1421–36.

74. Broon ND, Thompson FJ. Influence of fixation condi-tions on the performance of glutaraldehyde-treated por-cine aortic valves: towards a more scientific basis. Thorax. 1979;34:166–76.

75. Vesely I. The evolution of bioprosthetic heart valve de-sign and its impact on durability. Cardiovasc Pathol. 2003;12:177–86.

76. Yun KL, Miller DC, Moore KA, Mitchell RS, Oyer PE, Stinson EB, Robbins RC, Reitz BA, Shumway NW. Du-rability of the Hancock MO bioprosthesis compared with standard aortic valve bioprostheses. Ann Thorac Surg. 1995;60(Suppl.2):S221–S118.

77. Hilbert SL, Ferrans VJ. Porcine aortic valve bioprostheses: morphological and functional considerations. J Long-Term Eff Med Implants. 1992;2:99–112.

78. Zhon J, Fritze O, Schleicher M, Wendel HP, Schenke-Lay-land K, Haraztosi C, Hu S, Stock VA. Impact of heart valve decellularization on 3D ultrastructure, immunogenicity and thrombogenicity. Biomaterials. 2010;31:2549-–53.

79. Chicha I, Riffer A, Cesnjevaar R, Glöckler M, Agaimy A, Daniel WG, Garlichs CD, Dittrich S. Early obstructive of decellularized xegenic valves in pediatric patients: in-volvement of inflammatory and fibroproliferative process-es. Cardiovasc Pathol. 2011;20:222–31.

80. Zilla P, Zhang Y, Human P, Koen W, von Oppell V. Im-proved ultrastructural preservation of bioprosthetic tissue. J Heart Valve Dis. 1997;6:492–501.

81. Cigliano A, Gandaglia A, Lepedda AJ, Zinellu E, Naso F, Gastaldello A, Aguiari P, DeMuro P, Gerose G, Spina M, Formato M. Fine structure of glycosaminoglycans from fresh and decellularized porcine cardiac valves and peri-cardium. Biochem Res Int. 2012; article ID979351, 10 pp.

82. Cebotari S, Tudorache I, Jaekel T, Hilfiker A, Dorfman S, Ternes W, Hamerich A, Liditenberg A. Detergent decel-lularization of heart valves for tissue engineering: toxico-logical effects of residual detergents on human endothelial cells. Artif Organs. 2010;34:206–10.

83. Kasimir MT, Rieder E, Seebacher G, Nigisch A, Dekan B,

Wohrer E, Weigel G, Simon P. Decellularization does not eliminate thrombogenicity and inflammatory stimulation in tissue engineered porcine heart valves. J Heart Valve Dis. 2006;15:278–86.

84. Rieder E, Kasimir MT, Silberhumer G, Seebacher G, Wolner E, Simon P, Weigel P. Decellularization protocols of porcine heart valves differ importantly in efficiency of cell removal and susceptibility of the matrix to recelullarization with human vascular cells. J Thorac Cardiovasc Surg. 2004;127:399–405.